



City Research Online

City St George's, University of London

Citation: Athanassiadou, C. J., Karakostas, C. Z., Margaris, B. N. & Kappos, A. J. (2011). Displacement spectra and displacement modification factors, based on records from Greece. *Soil Dynamics and Earthquake Engineering*, 31(12), pp. 1640-1653. doi: 10.1016/j.soildyn.2011.06.008

This is the accepted version of the paper.

This version of the publication may differ from the final published version. To cite this item please consult the publisher's version.

Permanent repository link: <https://openaccess.city.ac.uk/id/eprint/13905/>

Link to published version: <https://doi.org/10.1016/j.soildyn.2011.06.008>

Copyright and Reuse: Copyright and Moral Rights remain with the author(s) and/or copyright holders. Copies of full items can be used for personal research or study, educational, or not-for-profit purposes without prior permission or charge, unless otherwise indicated, provided that the authors, title and full bibliographic details are credited, a hyperlink and/or URL is given for the original metadata page and the content is not changed in any way. For full details of reuse please refer to [City Research Online policy](#).

Displacement spectra and displacement modification factors, based on records from Greece

**C.J. ATHANASSIADOU², C.Z. KARAKOSTAS¹, B.N. MARGARIS¹, and A.J.
KAPPOS²**

¹Institute of Engineering Seismology & Earthquake Engineering, Thessaloniki, Greece

²Civil Engineering Department, Aristotle University of Thessaloniki, Greece

Abstract

Elastic and inelastic displacement spectra (for periods up to 4.0 sec) are derived, using a representative sample of acceleration records from Greece, carefully selected based on magnitude, distance and peak ground acceleration criteria, and grouped into three ground type categories according to the Eurocode 8 (EC8) provisions. The modification factor for the elastic design spectrum adopted in EC8 for accounting for damping is verified herein and is found to be satisfactory in the short to medium period range and less so in the long period range. The equivalent viscous damping ratio concept is also evaluated and is found to lead to underestimation of inelastic displacement spectra. Finally, based on the previously derived elastic and inelastic spectra, equations suitable for design and/or assessment purposes, are proposed for the corresponding displacement modification factors.

Keywords: displacement spectra, inelastic spectra, Eurocode 8, displacement modification factors, target displacement.

1. Introduction

During the last decade or so, a large emphasis has been placed on the proper evaluation of the displacement a structure will experience when subjected to an earthquake ground motion that is selected in the framework of design or assessment of the structure. This is mainly due to the fact that limit states (or performance objectives) for the structure can be conveniently

and meaningfully expressed in terms of displacements. There are two interrelated, still distinct, situations wherein estimation of displacements is a key issue.

First, in inelastic static (pushover) analysis, currently considered as a valuable tool for seismic assessment of structures, a target displacement is necessary for quantifying the seismic demand on the structure analysed [1, 2, 3]. This is typically evaluated on the basis of the maximum displacement of a single-degree-of-freedom (SDOF) system subjected to the ground motion(s) selected for assessment. The estimate of target displacement should account for the inelastic response of the structure as well as for the difference between the displacement of the SDOF system and that of the ‘monitoring point’ selected for the actual, multi-degree-of-freedom (MDOF), structure. The effect of inelasticity on the displacement of the SDOF system can be estimated either through an ‘equivalent linearization’ procedure, as in ATC-40 [2], or through a displacement modification factor that depends on ductility, as in ASCE-FEMA 356 [3].

In another situation, the so called ‘direct displacement-based’ design [4], or assessment [5], methods require reliable displacement spectra for a broad range of damping ratios, since the expected inelastic response of the structure is conveniently accounted for through a properly damped elastic spectrum and a ductility-dependent equivalent period of the structure (equivalent linearization approach); such elastic spectra for high damping ratios are also important for seismic isolation studies.

Previous works on elastic and inelastic displacement spectra so far concentrated on data sets from North America (e.g. [6], [7]), while (to the writers’ best knowledge) only one study was based on records mainly from Europe (Borzi et al. [8]). Although the dataset used in [8] is larger than the one used herein (it included records from all over Europe plus some from the Middle East), several of the records used herein were not included in [8]; notably, 24% of the records used in the present study are from earthquakes that occurred since 1999, a period not covered in the dataset of [8]. Furthermore, that previous study [8] has focussed on one particular version of displacement-based design method and derived the displacement modification factor in terms of the equivalent period of the inelastic system, rather than its initial one, which precludes comparisons with other similar studies such as [1], [6], [7]; in contrast, the present study addresses both the issue of elastic displacement spectra for several damping ratios and that of the displacement modification factor in terms of the initial period (common to both the elastic and the inelastic system) which is consistent with current trends worldwide and facilitates comparisons with previous studies.

In the study presented here, a carefully selected and properly processed sample of strong motion records from Greece (from 1978 to 2006) is used as a basis for the evaluation of both elastic and inelastic displacement spectra, using in-house developed software. Greece is the European Union country with the highest level of seismicity, while all kinds of seismotectonic environments are present in its territory, with fault mechanisms comprising normal, thrust and strike-slip types. Therefore, the results of the present study are of interest to all other European countries where consideration of seismic actions is pivotal in the design of new structures, as well as the assessment of existing structures. They are also useful for comparisons with the results of similar studies in America that involve larger datasets; some comparisons along these lines are included in sections 3 and 4 of this paper.

From statistical analysis of the elastic and inelastic spectra, modification factors for displacement (C_μ) are evaluated, and corresponding empirical relationships, suitable for design or assessment purposes, are proposed. Furthermore, the reduction factor for the elastic design spectrum adopted in EC8 for accounting for damping is verified in the light of the results of the present study and is found to be satisfactory.

2. Earthquake ground motions used

A key factor in studies like the present one is the proper choice of a representative sample among the available strong motion records in the area under consideration, in this work Greece. The sample compiled consists mainly of recordings from the permanent accelerometer network of the Institute of Engineering Seismology and Earthquake Engineering (ITSAK), which covers the entire Greek territory. Based on both international practice and the personal experience of the research team, the following criteria were applied in the selection of the acceleration time histories:

- Earthquake magnitude $M_w \geq 5.0$ and epicentral distance R from 5 km to 100 km.
- Value of peak ground acceleration $A_g \geq 0.10g$ and/or strong motion having caused non-negligible damage in the neighbourhood of the recording site.
- Availability of sufficient geotechnical data to classify existing ground conditions at the recording site according to the EC8 ground types [9].

Due to the relatively small number of records in the database, in some cases earthquakes of magnitude slightly less than 5.0 were selected, on condition that the amplitude of the horizontal motions was significant ($A_g > 0.10g$). The sample also includes records *THEA7802*, *KORA8101*, and *AMAA8805* that were recorded by the accelerometer network of the Institute

of Geodynamics, National Observatory of Athens (GINOA). The final record sample (75 accelerograms) used in the present study is an extended version of that used in a previous paper by Karakostas et al. [10], and is presented in Table 1.

It is worth noting that the sample includes some recently recorded ground motions. Of particular importance, as discussed in [10], is the January 8, 2006 strong earthquake (M=6.7) that occurred to the east of island of Kythira (South Aegean Sea); this was the first intermediate depth earthquake ever recorded in Greece (focal depth of 66 km), and it was found [10] to have a frequency content substantially different from that of previously recorded motions.

The processing of strong-motion data is carried out with a view to optimizing the balance between acceptable signal-to-noise ratio and information required for a particular application, both of which depend on the period and frequency content of the recording. In this study, analog and digital strong-motion data are included and for this reason some more advanced aspects of data processing are taken into account, enriching the frequency content of the aforementioned data. Recent applications of the data-processing methodology for analog strong-motion data used can be found in Margaris [11], Skarlatoudis et al. [12] and Athanassiadou et al. [13]. In those applications, models of noise in the digitized records were required and signal-to-noise ratios were estimated. For the digital strong-motion accelerograms (from digital instruments, which present several advantages compared to analog ones), signal-to-noise ratios were evaluated and the frequency ramps of the applied digital filters were determined. Due to the need for more reliable displacement time-histories, removal of the low-frequencies by filtering is attempted in such a way that little information meaningful for engineering purposes is lost. Recent data from several strong-motion events have shown that in displacement response spectra, the transition from the ascending to the horizontal branch of the spectrum occurs at significantly longer periods. Thus for the strong-motion data of this work and after the signal-to-noise ratio was estimated, a number of displacement time-histories were computed. Based on these, the final selection of the most appropriate low-frequency filtering was adopted [14], [15]. The high-pass filter cut-off frequency f_c employed for each record (that determines the maximum usable period for the record) is given in Table 1. It can be seen that the new filtering methodology permits the creation of response spectra that are reliable for periods up to 4.0 sec (in previous efforts, e.g. [10], the respective period limit was 2.5 sec). However, as can be seen from Table 1, 13 of the records of the selected earthquake sample have a cut-off frequency $f_c > 0.25$ Hz ($T < 4.0$ sec).

In Figure 1 the mean elastic (Fig. 1a) and inelastic (Fig. 1b) displacement spectra are presented, corresponding to the entire sample of 75 records or to the 62-record one (i.e. excluding the aforementioned 13 records). The spectra are plotted in a normalised form against T/T_g , where T_g is the predominant period of the ground motion, as will be further explained in the next chapter. As can be seen in Figure 1, the shape of the response spectra is practically the same in either case, although, as expected, the ordinates of the spectra of the reduced sample are higher in the long-period range. Since the focus of the present study is the *shape* of the response spectrum (not its amplitude), all results presented in the following are for the entire sample of 75 records (Table 1).

Using the geotechnical data available for each station, a ground classification according to the ground categories prescribed in EC8 [9] was carried out. A detailed presentation of the classification procedure can be found in [13]; the procedure is summarised in the remainder of this paragraph. In EC8 five basic ground types (A, B, C, D, E) and two special categories (S_1 and S_2) are defined, according to their stratigraphic profile and/or the value of the parameters $V_{S,30}$ (average shear wave velocity in the upper 30 meters of the ground), $NSPT$ (Standard Penetration Test blow-counts), and C_u (undrained shear strength). The sites of the selected recordings dataset are classified (Table 1) according to the value of $V_{S,30}$, wherever available; otherwise the values of $NSPT$, and alternatively of C_u (for cohesive soils), are used. In case none of the aforementioned parameters ($V_{S,30}$, $NSPT$, C_u) was available for the site of a recording station, categorization was based on a qualitative description of the stratigraphic profile and information from the corresponding geological map (IGME maps, scale 1:50,000). The recording stations were classified into three ground types: A (rock, $V_{S,30} > 800\text{m/s}$), B (very dense sand/gravel or very stiff clay, $360 < V_{S,30} \leq 800$) and C (dense or medium dense sand/gravel or stiff clay, $180 < V_{S,30} \leq 360$), as prescribed by EC8; no data was available for D or E sites, a situation common to that encountered in previous studies involving European records [10]. For the Preveza station (*PRE10301*) no geotechnical information was available; therefore, the two records have been used only for the computation of mean elastic and inelastic spectra irrespective of ground conditions (i.e. for the entire dataset). The remaining 73 records were classified as follows: 12 records in ground category A (16.4%), 33 records in ground category B (45.2%), and 28 records in ground category C (38.4%).

The spectra were evaluated, using the INELSP-2k program, for a period range from 0.01 to 4.0 sec, using a smaller step ($\Delta T = 0.025$ sec) for shorter periods ($T \leq 0.5$ sec), that gradually increases to $\Delta T = 0.50$ sec for $T > 3.0$ sec.

3. Elastic and inelastic spectra

As noted in the introduction, in displacement-based design (DBD) [4] and assessment [5], reliable displacement spectra are required for a broad range of damping ratios (up to about 30% or more); elastic spectra for high damping ratios are also important for seismic isolation studies. The need for such spectra in DBD arises from the fact that the *inelastic* displacement of the structure is represented by a properly damped *elastic* spectrum, wherein the amount of equivalent damping ratio (ζ_{eq}) is expressed as a function of the displacement ductility (μ) that the structure will experience when subjected to the considered level of earthquake. The idea of determining ζ_{eq} by equating the energy dissipated by hysteresis (area under force – displacement plot up to ductility μ) to the viscous damping energy (the area of the ellipse in the damping force vs. displacement plot) was put forward already in 1930 [16], while studies wherein ζ_{eq} was determined as a function of μ for several hysteresis models relevant to civil engineering structures appeared in the early 1980's [17]; the advent of DBD in the 1990's renewed the interest in the subject and relevant publications keep appearing to date (e.g. [18]). In a design situation, the foregoing spectrum is used to define (based on the selected design displacement) an equivalent period (also ductility-dependent) of the structure, which is then used to estimate the corresponding stiffness; in an assessment situation the equivalent period is used to estimate (again from the elastic spectrum for ζ_{eq}) the displacement that the (existing) structure will experience. In the following, the dataset of records from Greece is used to derive elastic displacement spectra for damping values within the period range relevant to DBD and seismic isolation applications.

3.1. Shape of elastic spectra

In Figure 2a the mean elastic displacement spectra for the entire sample are presented for various damping ratios ($0.02 \leq \zeta \leq 0.30$, where ζ is the viscous damping ratio). Separate plots are also given for the average spectra of records from earthquakes with $M_s > 5.5$ (“Type 1 spectra” according to EC8 provisions – Fig. 2b) and that of records from earthquakes with $M_s \leq 5.5$ (“Type 2 spectra” – Fig. 2c). In order to evaluate the spectral shape (that was the focus of this part of the study), rather than the absolute values of the spectral ordinates, all records were scaled according to the mean spectrum intensity (SI) of the entire sample. The spectral (or Housner) intensity is defined as the area under the pseudovelocity spectrum between 0.1 and 2.5 sec, and it has been found [e.g. 19] to be a very suitable scaling factor,

especially for periods longer than about 0.5 sec. Similar results have been obtained in the present research, as will be shown in the following.

As can be seen in Fig. 2, in the short period range the spectral displacements increase with period, with a tendency for stabilization after approximately a period of 0.8 sec for the entire sample, and beginning of a descending branch (for $\zeta \leq 10\%$ only) after a period of 2.0 sec (Fig. 2a). As expected, the influence of damping is more noticeable for lower values of ζ . The surface magnitude (M_s) seems to affect the maximum spectral displacements, which are significantly higher in the case of Type 1 spectra; it should be mentioned that numerical comparisons are meaningful here, as all accelerograms used in the calculation of the mean spectra of either Fig. 2b or Fig. 2c have been normalized to the same SI – the mean value of *the entire* sample. The effect of M_s on the shape of the derived spectra is even more significant. As can be seen in Fig. 2b, the spectral values in Type 1 spectra tend to increase for up to $T \approx 2.0$ sec (the rate of increase is smaller after $T \approx 0.65$ sec) and tend to decrease (for $\zeta \leq 10\%$) or to stabilize (for $\zeta > 10\%$) after the $T \approx 2.0$ sec threshold. On the other hand, Type 2 spectral values (Fig. 2c) tend to increase for up to $T \approx 0.75$ sec, after which they either start to decrease (for $\zeta \leq 10\%$) or to stabilize (for $\zeta > 10\%$).

In Fig. 3 mean elastic displacement spectra are presented either for the entire sample (Fig. 3a) or for each ground type (Figs. 3b, 3c and 3d, for EC8 ground types A, B and C, respectively). In each case the values were normalized to the mean SI either of the entire sample, or of the group of records pertaining to each ground type. The spectra are plotted against T/T_g , where T_g is the predominant period of the ground motion, which in this investigation is approximated by the period corresponding to the maximum peak of the respective elastic pseudovelocity spectrum for $\zeta=5\%$ [20]; site-dependent displacement spectra for essentially the same dataset of records in the usual format (i.e. plotted against T) can be found in [10]. It is noted that, whereas in displacement spectra plotted in the standard form, i.e. against T , ground conditions appear to affect the shape of the spectra (albeit to a lesser extent than they affect acceleration and velocity spectra) [10], this effect is less pronounced (as expected, on the basis of past studies) if the spectra are plotted in the normalized form, i.e. plotted against T/T_g .

The T_g value calculated for each record is shown in Table 1, while the mean T_g values for the entire sample and for ground type A, B and C (which were found to be 0.44 sec, 0.35 sec, 0.41 sec and 0.51 sec respectively) are shown in Fig. 3. As anticipated, T_g increases for softer

ground types, while the mean value for the entire sample was found to be very close to that of ground type B.

From Fig. 3 it is observed that the spectral displacements initially increase up to a period $T=T_g$, wherein a spectral peak appears, and then (for $\zeta < 10\%$) they decrease up to a period of $T \approx 1.5T_g$, after which they tend to stabilize. For $\zeta \geq 10\%$, the spectral displacements tend to stabilize for $T > 2T_g$. These trends generally hold for all spectral categories, irrespective of ground conditions, thus validating the argument that use of T/T_g in lieu of T is quite effective in eliminating the ground effect on the spectral shapes. This is seen even more clearly in Fig. 4, where the mean spectral displacements for the entire sample are plotted together with those of EC8 ground categories A, B and C. For comparison purposes, all spectra have been scaled to the same spectrum intensity (that of the entire sample). As can be seen from Fig. 4, the various spectral shapes are almost similar, with differences more accentuated in the $1 < T/T_g < 3$ range, which are nevertheless minor from an engineering point of view.

3.2. Evaluation of EC8 damping correction factor

An attempt was made to investigate the accuracy of the relationship proposed in EC8 [9] for the computation of design spectra for damping ratios $\zeta \neq 5\%$. EC8 suggests scaling of the design spectrum by a factor η given by

$$\eta = \sqrt{\frac{10}{5 + \zeta}} \geq 0.55 \quad (1)$$

In Figure 5, mean elastic displacement spectra are presented, derived from the entire record sample and for damping ratios $\zeta = 2, 10, 20$ and 30% , along with the corresponding spectra derived from the mean elastic spectrum for $\zeta = 5\%$ using the EC8 damping correction factor η . It is seen that the EC8 equation (1) slightly overestimates displacements in the short period range for $\zeta > 5\%$ (the overestimation increasing with ζ), whereas it underestimates displacements in the long period range ($T > 1\text{sec}$); overall, the agreement is deemed as satisfactory for relatively low damping ratios ($\zeta \leq 10\%$), and less so for higher ζ .

3.3. Shape of inelastic spectra

The next stage of the investigation consisted in the evaluation of inelastic displacement spectra, and the first issue addressed was the effect of scaling applied to the records. For the evaluation of the spectra, the modified Clough hysteresis model [22], a degrading stiffness model representative of the behaviour of well-designed reinforced concrete members [21],

was used, with a strain-hardening ratio of 5% and damping ratio $\zeta=5\%$. In Figure 6a the mean inelastic displacement spectra for the entire sample of records and for different ductility levels ($\mu=1.0$ – elastic behaviour, $\mu=2.0$ – low, $\mu=3.5$ – intermediate, and $\mu=5.0$ – high, ductility level) are normalized to a common spectrum intensity (mean SI of the sample), while in Figure 6b the spectra are normalized to a common peak ground acceleration value (PGA = 1.0 m/sec²). As can be seen from the figures, the shape of the inelastic displacement spectra does not seem to be substantially affected by the normalization method (whereas the values of the spectral ordinates do, see also [10]). In Figures 6c and 6d the corresponding coefficients of variation (COV) for each scaling method are plotted as a function of the period. Scaling according to SI seems to be very appropriate (in the sense that it reduces scatter) for periods T longer than about 0.4 sec (with COV less than 40% in this period range that is particularly relevant in displacement-based design). The respective COV values in the case of PGA-scaling are very satisfactory in the short period range (T less than about 0.3 sec); however the scatter increases significantly for longer periods, and while COV<1 for the whole period range examined (and tending to stabilize to a COV of about 80% for $T\geq 0.9$ sec), for $T>0.3$ sec the COV value for PGA-scaling is consistently higher than the respective one for SI normalization. The results are in line with conclusions of previous investigations [19], pointing out that SI-based scaling yields more reliable results, with the exception of very short periods. Given that for short periods displacements are typically not an issue, only the SI-based procedure was used in the remainder of this work.

While Figure 6a shows the mean inelastic displacement spectra (for various ductility levels, $1\leq\mu\leq 5.0$) for the entire sample of records (i.e. irrespective of earthquake magnitude), Figure 7a depicts the corresponding spectra for records classified as Type 1 according to EC8 (i.e. from earthquakes with $M_s > 5.5$) and Figure 7b the Type 2 spectra (earthquakes with $M_s \leq 5.5$). For comparison purposes, all spectra have been normalized to the mean SI of the entire sample. As can be seen from Fig. 6a, the ordinates of the mean inelastic displacement spectra for the entire sample increase up to a period of about 0.7sec and tend to stabilize at longer periods, but with lower ordinates compared to the respective elastic spectra. The spectral values tend to be lower for higher ductility levels, however the trend is not systematic and, overall, the effect of ductility level on the shape of inelastic displacement spectra is not significant. Similar comments apply to the EC8 Type 1 spectra (Fig. 7a), with the spectral values stabilizing after $T\approx 1.5$ sec. A different trend is observed for the EC8 Type 2 spectra (Fig. 7b), which show an ascending branch for periods up to about 0.7 sec, followed by a

descending one in the $0.7 < T < 1.5$ sec period range, after which the values tend to stabilize. The normalized ordinates of the inelastic displacement spectra for the higher surface magnitude (EC8 Type 1) records are significantly higher in the longer period ($T > 1.5$ sec) range, than the respective ones for lower magnitude (EC8 Type 2) earthquakes, an observation also made in the case of elastic displacement spectra.

The effect of ground conditions on the computed inelastic spectra is shown in Fig. 8, where the derived mean inelastic displacement spectra are shown either for the entire sample of records (Fig. 8a) or for EC8 ground type A (Fig. 8b), B (Fig. 8c) and C (Fig. 8d), as a function of the normalized period T/T_g . In each case, scaling was performed to the respective mean SI of the records involved. From Fig. 8 it can be seen that inelastic spectral displacements systematically increase up to $T=T_g$, irrespective of ground category. For higher T/T_g values – with the exception of soil C – displacements still increase but with a milder slope of the spectrum up to $T \approx 2.5T_g$, after which they tend to stabilize. In the case of soil C (Fig. 8d), stabilization initiates after the $T=T_g$ threshold. The minimization of the ground type effect on the spectral shape when the spectrum is plotted as a function of the normalized period T/T_g is once more demonstrated in Fig. 9, where the mean spectral displacements for each ground type, as well as for the entire sample, are plotted for the case $\mu=2$. For comparison purposes, all spectra have been scaled to the SI of the entire sample and a value of $T_g=0.44$ sec (i.e. that of the entire sample) was assumed. It is seen that the spectral shapes are reasonably similar, irrespective of ground conditions.

As mentioned previously, DBD presupposes the use of reliable ‘equivalent’ elastic spectra for damping ratios $\zeta > 5\%$, which are deemed to provide reasonable estimates of the corresponding inelastic displacements. In view of this, a comparison is made in Figure 10(a) between the mean *inelastic* displacement spectra for ground type B (for $\zeta=5\%$ and $2 \leq \mu \leq 5.0$) with the respective mean elastic spectra for an equivalent damping ratio ζ_{eq} calculated as suggested by Kappos [17] on the basis of equal energy dissipation approach [16] and the modified Clough hysteresis model [22]

$$\zeta_{eq} = \frac{1}{\pi} \frac{(1-p)(\mu-1)}{\mu} \quad (2)$$

where $p=0.05$ is the strain-hardening ratio and μ the displacement ductility. Although the hysteresis model is the same degrading stiffness one used for deriving inelastic spectra (through the rigorous method), it can be seen from Fig. 10(a) that the use of equation (2) leads to underestimation of displacement values, particularly for higher ductility values.

A similar comparison was also made using the more recent, period-dependent, relationship for the equivalent damping ratio proposed by Dwairi et al. [18] for ‘Large Takeda-type’ hysteretic behaviour (very similar to that of the model [22] used herein):

$$\zeta_{eq} = \zeta_v + C_{LT} \left(\frac{\mu - 1}{\pi \mu} \right) \quad (3)$$

Where ζ_v is the damping ratio in the elastic range (5%),

$$C_{LT} = 65 + 50 (1 - T_{eff}) \quad \text{for } T_{eff} < 1 \text{ sec}$$

$$C_{LT} = 65 \quad \text{for } T_{eff} \geq 1 \text{ sec}$$

and

$$\frac{T_{eff}}{T_i} = \sqrt{\frac{\mu}{1 + p\mu - p}} \quad (4)$$

with p and μ denoting the strain-hardening ratio and μ the displacement ductility. The results are presented in Fig. 10(b) and are similar to those obtained using expression (1) for the equivalent damping ratio (Fig. 10(a)), which is easier to apply since constant ζ is used along the entire period range. A much clearer picture of the discrepancies between the inelastic and equivalent elastic spectra (using equations (2) and (3)), is given in Table 2. The general trend is that the underestimation of inelastic spectral ordinates is substantial in the short period range ($T < 0.5s$) and much more important in the case of high ductility (in the critical case of $T = 0.1s$, the underestimation is up to 69% for $\mu = 5.0$, and up to 44% for $\mu = 2.0$); however, this period range is hardly relevant for DBD, so there are really no practical repercussions of the aforementioned underestimation. The real practical concern is that even in the long period range there is some underestimation, rather insignificant for $\mu = 2.0$ (about 10%), but significant for $\mu = 5.0$ (up to 27% for $T = 1.0$, and up to 15% for $T = 3.0s$). Hence, the overestimation of the equivalent damping - and consequently the underestimation of inelastic displacements - by the ζ_{eq} approach, is confirmed for both approaches studied here (based on ζ_{eq} equations proposed in [17] and [18]), making it a point of concern regarding the proper application of DBD procedures.

4. Evaluation of displacement modification factors

The displacement modification factor C_μ (coefficient C_I in FEMA356 [3]) is defined as the ratio of the ordinate of the inelastic displacement spectrum for a given period to the corresponding elastic value:

$$C_\mu(T) = \frac{S_{d,in}(T)}{S_{d,el}(T)} \quad (5)$$

The displacement modification factors C_μ evaluated using the elastic and inelastic spectra derived in this study are shown in Figure 11 for the entire sample of records (Fig. 11a), for EC8 Type 1 (Fig. 11b) and Type 2 (Fig. 11c) earthquakes, for different ductility levels and $\zeta=5\%$ damping. For comparison purposes, scaling to the mean SI of the entire sample was performed. As expected, the value of C_μ is significantly greater than 1 in the short period range (with higher values for increasing ductility μ), while for $T \geq T_i$ it tends to stabilize to a value of about unity. The value of T_i is found to be dependent on the ductility level, especially for lower ductility values. For example it is found that for the entire sample (Fig. 11a) $T_i = 0.22, 0.36$ and 0.39 sec for $\mu=2.0, 3.5$ and 5.0 respectively. The respective values for Type 1 spectra (Fig. 11b) are found to be $T_i = 0.23, 0.40$ and 0.41 sec and for Type 2 spectra (Fig. 11c) $T_i = 0.17, 0.34$ and 0.345 sec. In the very short period range, as discussed, values of C_μ are significantly greater than 1, and they agree to a satisfactory degree with the observation made by other researchers (e.g. Miranda [23]), that for $T \rightarrow 0$ $C_\mu \rightarrow \mu$. Moreover, it is noted that earthquake magnitude (Fig. 11b vs. 11c) does not seem to affect this general trend.

In Figure 12, the computed C_μ values are shown as a function of the T/T_g ratio either for the entire sample of records (Fig. 12a) or for EC8 ground types A (Fig. 12b), B (Fig. 12c) and C (Fig. 12d). For the derivation of these results, the corresponding records were scaled to the SI of the pertinent ground category. From the spectra of Fig. 12 it appears that ground type does not affect the general trend of the displacement modification factor. For the entire sample, as well as for each ground type, the equal displacement approximation (equality of inelastic and elastic displacements) seems to be valid for periods longer than $T \approx 1.5T_g$ (with corresponding values $T_g = 0.44, 0.35, 0.41$ and 0.51 sec for the entire sample and each ground type, respectively). Hence, it is confirmed that plotting the displacement modification factor in terms of T/T_g tends to alleviate ground type effects. This can also be seen in Fig. 13, where the mean C_μ for the entire sample, as well as the three ground categories, are plotted for the

$\mu=2.0$ case. A close similarity among the computed displacement modification factors, irrespective of ground category, can be observed.

Evaluation of an analytical relationship for C_μ as a function of period T and ductility μ is useful for design and assessment purposes. From its definition (eq. 5), it is obvious that for elastically behaving systems, the value of C_μ should be :

$$C_\mu(T, \mu_i = 1) = 1 \quad (6)$$

Already from the first attempts for the evaluation of inelastic displacement spectra (e.g Veletsos & Newmark [24]), it was observed that in the long period range ($T > 1\div 2$ sec), the spectral displacements of elastic and inelastic systems were practically the same, i.e. the following condition holds :

$$C_\mu(T \rightarrow \infty, \mu_i) = 1 \quad (7)$$

In the medium and short period range, inelastic displacements depend largely on the period of the system, and especially in the very short period range, inelastic displacements are significantly larger than the corresponding elastic ones.

It is also noted that the displacement modification factor can be expressed as

$$C_\mu = \frac{\Delta_{in}}{\Delta_{el}} = \frac{\mu \cdot \Delta_y}{\Delta_{el}} = \frac{\mu \cdot R_{el}}{R_y} = \frac{\mu}{q_\mu} \quad (8)$$

where Δ_{in} and Δ_{el} are the peak displacements of an SDOF oscillator with inelastic and elastic response, respectively, Δ_y is the yield displacement, R_y and R_{el} are the corresponding inelastic (yield) and elastic strength and $q_\mu = \frac{R_{el}}{R_y}$ is the ductility-dependent component of the behaviour factor [21].

In an earlier work ([10]) on design spectra and strength modification factors based on an almost identical record dataset from Greece (the difference is explained later), the authors proposed the following equation for q_μ :

$$q_\mu = \frac{1}{F + \frac{G}{\mu} + H(\ln T)^2} \quad \text{for } 1 < \mu \leq 5, \quad 0.025 \leq T \leq 2.5 \text{ sec} \quad (9)$$

together with suitable values for the coefficients F , G and H either for the entire dataset, or for each different ground type subset, as shown in Table 3.

Based on the limit conditions mentioned above, taking into account relationships (6) and (7), and the fact that in this study spectra were derived up to $T \approx 4$ sec, the following equation is proposed for the displacement modification factor C_μ :

$$C_\mu = F\mu + G + H \mu(\ln T)^2 \quad \text{for } 1 < \mu \leq 5, \quad 0.025 \leq T \leq 4.0 \text{ sec} \quad (10a)$$

$$C_\mu = 1 \quad \text{for } 1 < \mu \leq 5, \quad T > 4.0 \text{ sec} \quad (10b)$$

A best-fit procedure has been applied to find the relevant values of coefficients F , G and H for the various C_μ cases that were derived from the earthquake dataset used in this study. It is recalled that the dataset used herein, differs from that used in [10] in that it includes the records of the intermediate-depth Kythira earthquake (Table 1, event 26, records 72÷75), while this particular earthquake was treated as a separate, special, case in [10]. It is the first intermediate-depth earthquake recorded in Greece, and its spectral characteristics are markedly different (much richer in the medium period range i.e. from about 0.4 to 1.3 sec) from those of the other, shallow-depth, earthquakes of the dataset (whose spectral peaks typically appear in the short period range, i.e. for periods less than about 0.3 sec). Therefore, the inclusion of the Kythira earthquake in the present dataset affects considerably the results for EC8 ground types A and B compared to those obtained in [10] for the same ground types.

In Table 4, the corresponding values for coefficients F , G and H are presented for the entire earthquake dataset, as well as for each specific case of Type 1 and Type 2 response spectra (see Fig. 10a-c).

A similar analysis was carried out for each EC8 ground type case and the results are presented in Table 5. In all cases, fitting was made using T (not T/T_g) as an independent parameter, in order to be compatible with equation (8). The authors believe that the proposed equations are more readily applicable in civil engineering practice, since they require knowledge of only the ground classification at a site, not of the corresponding T_g . If deemed necessary, a transformation of the obtained analytical results from a function of T to a function of T/T_g is straightforward.

By comparing the obtained values for the coefficients F , G and H proposed for q_μ in [10] for the entire dataset (first column of Table 3) and those obtained from the –not identical, as described above- earthquake dataset of the present study for C_μ (first column of Table 4) it can be seen that they are very similar. This conclusion is even more supported by the almost identical coefficient values for EC8 ground type C (which comprises the same earthquake

records in both the present dataset and that of [10], see last columns of Tables 3 and 5). This does not hold for the corresponding results for ground type A, since ground type A dataset comprises very few records and the inclusion (or otherwise) of the Kythira earthquake substantially affects the final results. However, the Kythira earthquake does not significantly influence the coefficients for the case of the more populated ground type B dataset (see Tables 3 and 5). Therefore, one can use the same set of numerical coefficients F , G and H of Tables 4 and 5 either in equation (9) for the estimation of q_μ or in equation (10) for estimation of C_μ .

Finally, in the last rows of Tables 4 and 5, the correlation coefficient r^2 between the proposed equation and the actual data is given. Good agreement is observed in all cases between the observed data and those predicted from equation (10).

In Fig. 14, a 3D and a 2D graph of the actual data and the proposed analytical relationship for C_μ (eq. (8)) are presented for the case of the entire record sample. From the graphs, it is clear that the proposed relationship (8a) satisfies to an acceptable degree limit condition (5). Also, use of the proposed relationship will be necessary in practice only for $\mu > 1$, but in any case, it is clear from the graphs that it fulfils also, to a certain degree, limit condition (4) for the elastic behaviour ($\mu=1$) case in the $0.2 < T < 4$ sec period range. Similar conclusions were also found to hold for all other C_μ results for various subsets of the entire sample examined herein (i.e. for EC8 Type 1 and 2 earthquakes or ground-type specific cases).

5. Conclusions

From the analyses performed within the framework of the present study, the following conclusions can be drawn:

1. In the case of elastic displacement spectra, the surface magnitude (M_s) was found to affect the maximum spectral displacements and particularly the spectral shapes, as can be seen from the derived mean spectra for Type 1 and Type 2 earthquakes (according to EC8).
2. Ground conditions appear to affect the shape of the elastic displacement spectra (albeit to a lesser extent than they affect acceleration and velocity spectra). However, this effect is much less pronounced if the spectra are plotted against the normalized period T/T_g .
3. Use of the scaling factor η prescribed in EC8 for the calculation of elastic spectra for damping ratios $\zeta \neq 5\%$ leads to results that agree overall quite well with the directly

computed spectra, especially for relatively low damping ratios ($\zeta \leq 10\%$). However, the EC8 factor leads to underestimation of the spectral ordinates in the long period range (about 1 to 2 sec, depending on the amount of damping).

4. The normalization method applied to the computed mean inelastic displacement spectra (scaling to either SI or PGA), does not seem to substantially affect the spectral shapes (whereas it does affect the values of the spectral ordinates). It is nevertheless found that scaling to SI seems to be very appropriate (in the sense that it reduces scatter) for periods longer than about 0.4 sec (a period range relevant to displacement-based design).
5. The overall effect of ductility level on the ordinates of inelastic spectral displacements is not significant. The normalized spectral inelastic displacement values for the higher magnitude (EC8 Type 1) records are significantly higher than the respective ones for lower magnitude (Type 2) earthquakes, an observation also made in the case of elastic displacement spectra.
6. As in the case of elastic, also for inelastic displacement spectra the effect of ground conditions is less pronounced if the spectra are plotted against T/T_g .
7. Use of an equivalent damping ratio ζ_{eq} for the computation of inelastic displacement spectra from 'equivalent' elastic ones leads to underestimation of the displacements due to an overestimation of the equivalent damping proportional to the ductility level.
8. Displacement modification factors C_μ evaluated using the derived elastic and inelastic spectra are found to be very little affected by the ductility level. Also, the earthquake magnitude does not seem to have a noticeable effect on the computed C_μ curves. Plotting C_μ in terms of T/T_g seems to alleviate ground type effects on the shape of the curve (as was also the case for the elastic and inelastic displacement spectra).
9. An analytical relationship was proposed for the computation of the displacement modification factor in terms of period, ductility level, and ground type. The proposed equation is theoretically compatible to one proposed for the force reduction (behaviour) factor in an earlier study by the writers. Hence, the same coefficients can be used in either equation for the computation of either the force or the displacement modification factors.

Acknowledgements

The authors would like to acknowledge the contribution of Dr. N. Klimis, former ITSAK Researcher and presently Associate Professor at the Democritus University of Thrace, Greece, to the ground classification of the records during an earlier research effort.

References

1. FEMA. Improvement of nonlinear static seismic analysis procedures (FEMA-440/ATC-55). FEMA-NEHRP, 2005.
2. Applied Technology Council. ATC-40: Seismic evaluation and retrofit of concrete buildings. Rep. SSC 96-01, CSSC-ATC, Redwood City, Calif., 1996.
3. ASCE (American Society of Civil Engineers) (2000) Prestandard and Commentary for the Seismic Rehabilitation of Buildings, FEMA, Washington DC, Nov. (FEMA 356).
4. Kowalsky, MJ, Priestley, MJN and MacRae, GA. Displacement-based design of RC bridge columns in seismic regions. *Earthquake Engineering & Structural Dynamics* 1995; 24 (12), 1623-1643.
5. Priestley, MJN. Displacement-based seismic assessment of reinforced concrete buildings, *Journal of Earthquake Engineering* 1997; 1 (1), 157-192.
6. Miranda, E. Estimation of inelastic deformation demands of SDOF systems, *Journal of Structural Engineering*, ASCE 2001; 127 (9): 1005 – 1012.
7. Miranda, E and Ruiz-Garcia, J. Evaluation of approximate methods to estimate maximum inelastic displacement demands, *Earthquake Engineering & Structural Dynamics* 2002; 31:539–560.
8. Borzi, B, Calvi, GM, Elnashai, AS, Faccioli, E, and Bommer, JJ. Inelastic spectra for displacement-based seismic design; *Soil Dynamics & Earthquake Engineering* 2001; 21 (1), 47-61.
9. CEN (Comité Européen de Normalisation). Eurocode 8: Design of structures for earthquake resistance – Part 1: General rules, seismic actions and rules for buildings (EN 1998-1: 2004), Brussels, May 2004.
10. Karakostas, CZ, Athanassiadou, CJ, Kappos, AJ and Lekidis, VA. Site-dependent design spectra and strength modification factors, based on records from Greece, *Soil Dynamics & Earthquake Engineering* 2007; 27:1012-1027.

11. Margaris BN. New fast digitization and correction procedures of the Greek strong motion records. In: Proceedings of XXIV General Assembly of the European Seismological Commission Vol. II : Athens, Sept 19-24, 1994; 779-786.
12. Skarlatoudis, AA, Papazachos, CB, & Margaris, BN. Determination of noise spectra from strong motion data recorded in Greece. *Journal of Seismology* 2003; 7:533-540.
13. Athanassiadou, C, Kappos, A, Karakostas, C, Klimis, N, Lekidis, V, Margaris, V, and Theodulidis, N. Elastic and inelastic spectra for Greek earthquakes, based on a representative set of records. In: Proceedings of the 5th International Conference on Earthquake Resistant Structures (ERES2005), Skiathos, Greece, May 30 - June 1, 2005; 733-743.
14. Boore, D. M. Analog-to-digital conversion as a source of drifts in displacements derived from digital recordings of ground acceleration. *Bulletin of Seismological Society of America*, 2003; 93: 2017-2024.
15. Skarlatoudis A., Margaris, B. “The Kythera earthquake 08/01/2006: processing of records from different digital sensors and high-pass filtering effects in source simulations”. In: Proceedings of 3rd Hellenic Conference of Earthquake Engineering & Engineering Seismology, Athens, Nov. 5-7, 2008, Paper No 1790 (in Greek).
16. Jacobsen, LS. Steady forced vibrations as influenced by damping, *ASME Transactions* 1930; 52(1), 169–181.
17. Kappos, AJ. Damping Parameters in Computer-Aided Seismic Analysis of R/C Buildings”, *International Conference on Computer-Aided Analysis and Design of Concrete Structures*, Split, Yugoslavia, Sep. 1984; Part I, 231-244.
18. Dwairi, HM, Kowalsky, MJ, and Nau, JM. Equivalent Damping in Support of Direct Displacement-Based Design, *Journal of Earthquake Engineering* 2007; 11(4): 512–530.
19. Kappos AJ, Kyriakakis P. A reevaluation of scaling techniques for natural records. *Soil Dynamics and Earthquake Engineering* 2000; 20(1–4):111–23.
20. Miranda, E. Evaluation of site-dependent inelastic seismic design spectra, *Journal of Structural Engineering*, ASCE 1993; 119 (5): 1319-1338.
21. Kappos, AJ. Evaluation of behaviour factors on the basis of ductility and overstrength studies. *Engineering Structures* 1999; 21(9): 823-835.
22. Riddell, R. and Newmark, N.M. Force-deformation models for nonlinear analyses, (Technical Note), *Journal of Structural Division ASCE* 1979; 105 (ST12): 2773-2778.

23. Miranda, E. Inelastic displacement ratios for structures on firm sites. Journal of Structural Engineering ASCE 2000; 126(10): 1150-1159.
24. Veletsos, A. S., Newmark, N.M. "Effect of inelastic behavior on the response of simple systems to earthquake motions". In : Proceedings of 2nd World Conference on Earthquake Engineering. 2: 895-912, 1960.

Table 1. Characteristics of records used in the present study

	Event	Date	Or. Time	Lat	Long	M _w	Epice ntral distan ce	Record identifier	MP	Instrum ent Instal. *	Soil categ EC8	α_g (cm/sec ²)	f _c (Hz)	T _g (sec)
1	1	062078	200321	40.8	23.2	6.5	26	THEA7802	L	B	C	143.90	0.20	0.940
2						6.5	26	THEA7802	T			148.57	0.20	0.500
3	2	022481	205338	38.22	22.93	6.7	32	KORA8101	L	B	C	235.01	0.15	0.790
4						6.7	32	KORA8101	T			290.62	0.15	0.870
5	3	011783	124129	38.09	20.19	7.0	35	ARG18301	L	B	B	169.22	0.25	0.890
6						7.0	35	ARG18301	T			140.99	0.25	0.470
7	4	032383	235106	38.33	20.22	6.2	26	ARG18307	L	B		173.49	0.25	0.160
8						6.2	26	ARG18307	T			223.40	0.25	0.200
9	5	032483	041732	38.18	20.32	5.4	22	ARG18308	L	B		250.31	0.35	0.160
10						5.4	22	ARG18308	T			280.88	0.35	0.180
11	6	082683	125210	40.51	23.92	5.1	47	POL18302	L	B	A	92.49	0.50	0.160
12						5.1	47	POL18302	T			50.80	0.50	0.230
13	7	102584	094916	36.83	21.71	5.0	9	PEL18401	L	FF	A	168.34	0.20	0.290
14						5.0	9	PEL18401	T			176.78	0.20	0.320
15	8	091386	172434	37.03	22.2	6.0	12	KAL18601	L	B	B	229.92	0.10	0.650
16						6.0	12	KAL18601	T			263.69	0.10	0.670
17	9	091586	114130	37.04	22.13	5.3	3	KAL18608	L	B		233.03	0.15	0.700
18						5.3	3	KAL18608	T			138.38	0.15	0.570
19						5.3	3	KAL28602	L	B	B	157.84	0.30	0.560
20						5.3	3	KAL28602	T			255.20	0.10	0.670
21	10	101688	123406	37.95	20.9	6.0	20	ZAK18804	L	B	C	134.57	0.20	0.530
22						6.0	20	ZAK18804	T			146.66	0.20	0.560
23						6.0	28	AMAA8805	L	B	C	84.11	0.20	0.520
24						6.0	28	AMAA8805	T			156.94	0.20	0.450
25	11	122190	065744	40.98	22.34	6.0	32	EDE19001	L	B	C	100.88	0.20	0.680
26						6.0	32	EDE19001	T			95.07	0.20	0.710
27	12	032693	114516	37.66	21.39	4.9	6	PYR19306	L	B	C	108.47	0.25	0.420
28						4.9	6	PYR19306	T			218.14	0.25	0.170
29	13	032693	115613	37.69	21.43	4.9	10	PYR19307	L	B		99.20	0.35	0.210
30						4.9	10	PYR19307	T			118.03	0.35	0.320
31	14	032693	115815	37.49	21.49	5.4	14	PYR19308	L	B		166.34	0.20	0.400
32						5.4	14	PYR19308	T			430.47	0.20	0.410
33	15	071493	123149	38.24	21.78	5.6	10	PAT19302	L	B	C	146.22	0.20	0.440
34						5.6	10	PAT19302	T			197.95	0.20	0.800
35						5.6	9	PAT29302	L	FF	C	166.19	0.25	0.390
36						5.6	9	PAT29302	T			404.42	0.25	0.340

37	16	050495	003411	40.54	23.63	5.3	26	POL19506	L	B	A	142.65	0.45	0.150
38						5.3	26	POL19506	T			102.72	0.45	0.180
39	17	051395	084715	40.16	21.67	6.6	16	KOZ19501	L	B	A	209.87	0.25	0.250
40						6.6	16	KOZ19501	T			139.91	0.25	0.340
41	18	051595	041357	40.07	21.67	5.1	13	CHR19513	L	FF	B	159.48	0.15	0.160
42						5.1	13	CHR19513	T			131.93	0.15	0.210
43	19	051795	041426	40.07	21.61	5.3	11	CHR19532	L	FF		117.43	0.10	0.540
44						5.3	11	CHR19532	T			130.36	0.10	0.240
45	20	051995	064850	40.03	21.62	5.1	12	KRR19501	L	FF	B	185.14	0.15	1.000
46						5.1	12	KRR19501	T			262.10	0.15	0.400
47	21	061195	185195	39.96	21.58	4.8	5	KRR19509	L	FF		120.17	0.15	0.430
48						4.8	5	KRR19509	T			82.95	0.15	0.400
49						4.8	7	KEN19563	L	FF	C	125.07	0.10	0.560
50						4.8	7	KEN19563	T			99.81	0.10	0.500
51	22	080596	224642	40.06	20.66	5.7	8	KON29601	L	B	C	383.14	0.10	0.450
52						5.7	8	KON29601	T			381.91	0.10	0.400
53						5.7	8	KON19601	T	B	B	168.32	0.10	0.790
54	23	111897	130753	37.33	20.84	6.6	48	ZAK19703	L	B	C	114.28	0.15	0.430
55						6.6	48	ZAK19703	T			130.61	0.15	0.910
56	24	090799	115651	38.15	23.62	5.9	20	ATH29901	L	B	B	109.60	0.35	0.360
57						5.9	20	ATH29901	T			161.52	0.35	0.220
58						5.9	15	ATH39901	L	B	B	259.52	0.20	0.690
59						5.9	15	ATH39901	T			303.34	0.20	0.230
60						5.9	17	ATH49901	L	B	A	119.43	0.20	0.480
61						5.9	17	ATH49901	T			109.61	0.20	0.480
62						5.9	15	KERT9901	L	B	B	216.95	0.40	0.530
63						5.9	15	KERT9901	T			182.31	0.40	0.220
64						5.9	36	RFNA9901	L	FF	B	83.82	0.25	0.580
65						5.9	36	RFNA9901	T			103.62	0.25	0.460
66						5.9	14	SPLB9901	L	B	B	345.83	0.10	0.260
67						5.9	14	SPLB9901	T			319.86	0.10	0.290
68	25	081403	051454	38.76	20.60	6.2	12	LEF10301	L	B	C	334.48	0.10	0.690
69						6.2	12	LEF10301	T			409.94	0.10	0.540
70						6.2	24	PRE10301	L	B	N/A	153.20	0.10	0.410
71						6.2	24	PRE10301	T			141.04	0.10	0.580
72	26	010806	113454	36.21	23.41	6.9	40	KYT10601	L	FF	A	120.96	0.07	0.660
73						6.9	40	KYT10601	T			103.97	0.07	0.760
74						6.9	41	ANS10601	L	FF	B	144.25	0.10	0.560
75						6.9	41	ANS10601	T			66.74	0.10	0.435

* **'Instrument Instal.:** The location where the accelerographic instrument is installed

B: Basement of building with two or more storeys

FF: Free-Field (storage area or shelter or small 1-storey building).

Table 2. Comparisons of S_d values (in mm) from inelastic and elastic (for $\zeta=\zeta(\mu)$) spectra

μ	T (sec)	$S_{d,inel}$	$S_{d,el}$ (Kappos ζ_{eq})	$S_{d,el}$ (Dwairi ζ_{eq})	[(3)-(4)]/(3)	[(3)-(5)]/(3)
(1)	(2)	(3)	(4)	(5)	(6)	(7)
2.0	0.1	1.761	1.116	0.987	-0.3663	-0.4395
	0.3	9.073	6.955	6.181	-0.2334	-0.3187
	0.5	14.834	11.379	10.573	-0.2329	-0.2872
	0.7	18.709	15.156	14.950	-0.1899	-0.2009
	1.0	18.007	16.315	16.223	-0.0940	-0.0991
	2.0	22.240	19.754	19.659	-0.1118	-0.1161
	3.0	21.125	19.162	19.096	-0.0929	-0.0960
3.5	0.1	2.366	0.996	0.898	-0.5790	-0.6205
	0.3	9.532	5.980	5.563	-0.3726	-0.4164
	0.5	14.499	9.661	9.765	-0.3337	-0.3265
	0.7	15.356	12.874	13.431	-0.1616	-0.1254
	1.0	17.471	14.102	14.630	-0.1928	-0.1626
	2.0	20.174	17.537	18.078	-0.1307	-0.1039
	3.0	20.094	17.583	17.965	-0.1250	-0.1060
5.0	0.1	2.845	0.959	0.871	-0.6629	-0.6938
	0.3	10.378	5.666	5.419	-0.4540	-0.4778
	0.5	14.684	9.127	9.671	-0.3784	-0.3414
	0.7	15.688	12.153	12.887	-0.2253	-0.1785
	1.0	18.347	13.425	14.116	-0.2683	-0.2306
	2.0	20.148	16.824	17.549	-0.1650	-0.1290
	3.0	20.046	17.105	17.592	-0.1467	-0.1224

Table 3. Coefficients previously proposed for q_{μ} (eq. 9)

	Entire sample	Soil type A (EC8)	Soil type B (EC8)	Soil type C (EC8)
F	-0.0349	-0.0668	-0.0373	-0.0297
G	0.9183	0.9561	0.9153	0.9144
H	0.0479	0.0426	0.0463	0.0499

Table 4. Coefficients and correlation coefficients for proposed equations for C_{μ} (eq. 10)

	Entire sample	Type 1 (EC8)	Type 2 (EC8)
F	-0.0316	-0.0312	-0.0322
G	0.9136	0.9011	0.9280
H	0.0472	0.0502	0.0437
$r^2 (C_{\mu})$	0.8816	0.8484	0.8962

Table 5. Coefficients and correlation coefficients for proposed equations for C_{μ} (eq. 10)

	Soil type A (EC8)	Ground type B (EC8)	Ground type C (EC8)
F	-0.0277	-0.0359	-0.0271
G	0.9198	0.9141	0.9104
H	0.0418	0.0463	0.0487
$r^2 (C_{\mu})$	0.8544	0.8839	0.8642

FIGURE CAPTIONS

Fig. 1. Mean spectra for the entire sample and the reduced one not including the 13 records with $f_c \geq 0.25$ Hz: (a) elastic spectra, (b) inelastic spectra.

Fig. 2. Mean elastic displacement spectra: (a) entire sample, (b) $M_s > 5.5$, (c) $M_s \leq 5.5$.

Fig. 3. Mean elastic displacement spectra: (a) entire sample, (b) ground type A, (c) ground type B, (d) ground type C.

Fig. 4. Mean elastic displacement spectra (for $\zeta = 5\%$)

Fig. 5. Comparison between mean elastic displacement spectra and those derived from the EC8-prescribed values of the damping correction factor (entire sample).

Fig. 6. Mean inelastic displacement spectra: (a) scaled to the mean spectrum intensity SI, (b) scaled to the same peak ground acceleration PGA ($a_g = 1.0$ m/sec²), (c) COV for the same SI case, (d) COV for the same PGA case.

Fig. 7. Mean inelastic displacement spectra: (a) Type 1 ($M_s > 5.5$), (b) Type 2 ($M_s \leq 5.5$).

Fig. 8. Mean inelastic displacement spectra: (a) entire sample, (b) ground type A, (c) ground type B, (d) ground type C.

Fig. 9. Mean inelastic displacement spectra ($\mu = 2.0$)

Fig. 10. Comparison between mean inelastic displacement spectra with $\zeta = 5\%$ and elastic ones with $\zeta = \zeta(\mu)$ for ground type B.

Fig. 11. Mean displacement modification factors: (a) entire sample, (b) $M_s > 5.5$, (c) $M_s \leq 5.5$.

Fig. 12. Mean displacement modification factors: (a) entire sample, (b) ground type A, (c) ground type B, (d) ground type C.

Fig. 13. Mean displacement modification factors ($\mu = 2.0$)

Fig. 14. Proposed displacement modification factor C_μ as function of T and μ (eq.(8)) - entire sample : (a) 3-D and (b) 2-D representation.

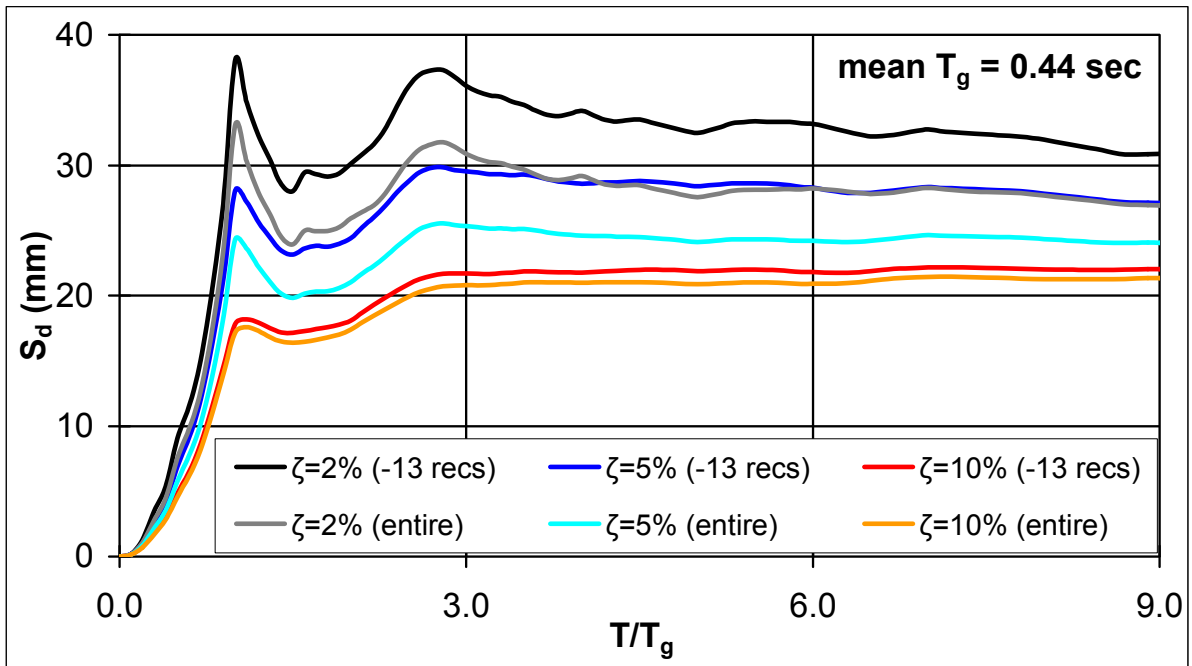


Fig. 1 (a)

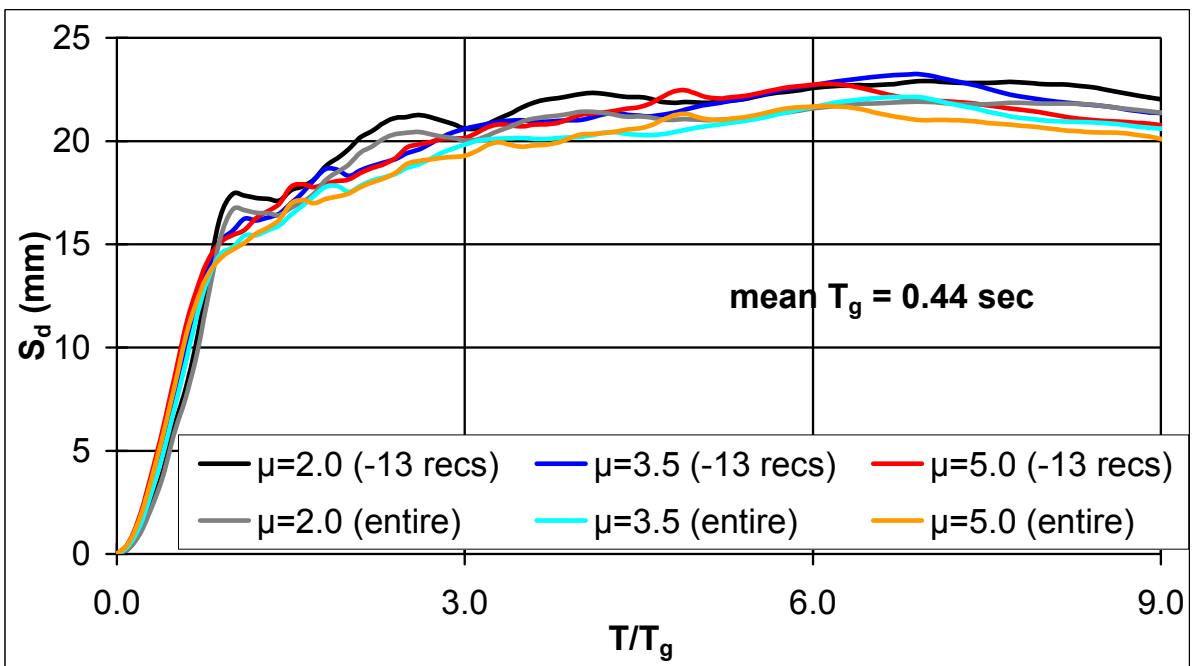


Fig. 1 (b)

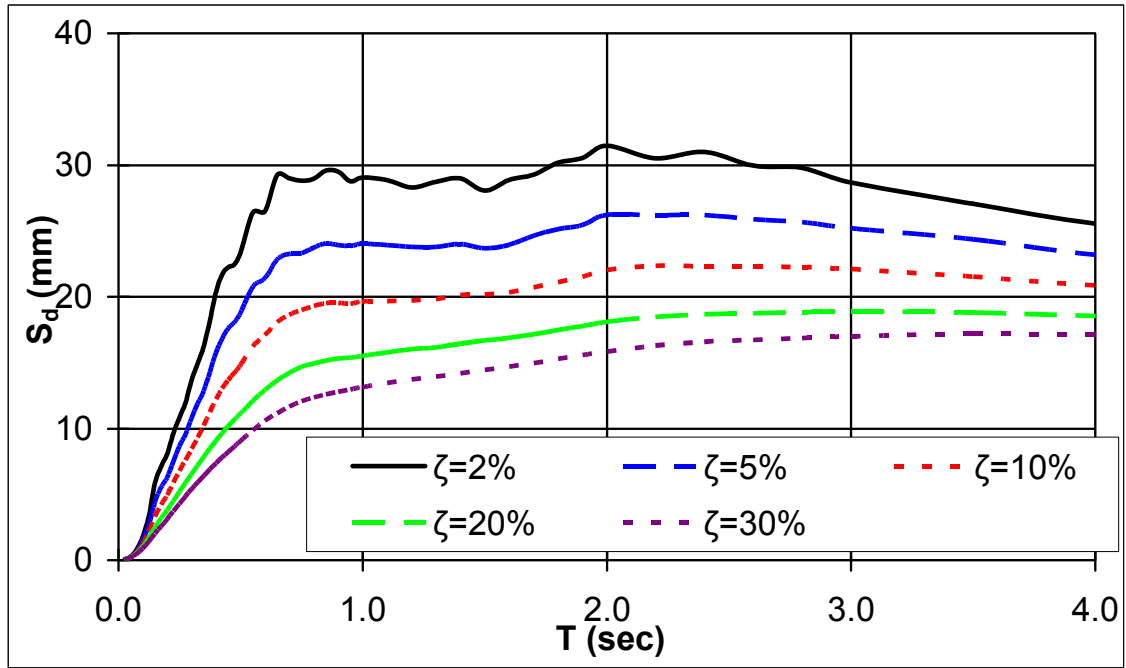


Fig. 2 (a)

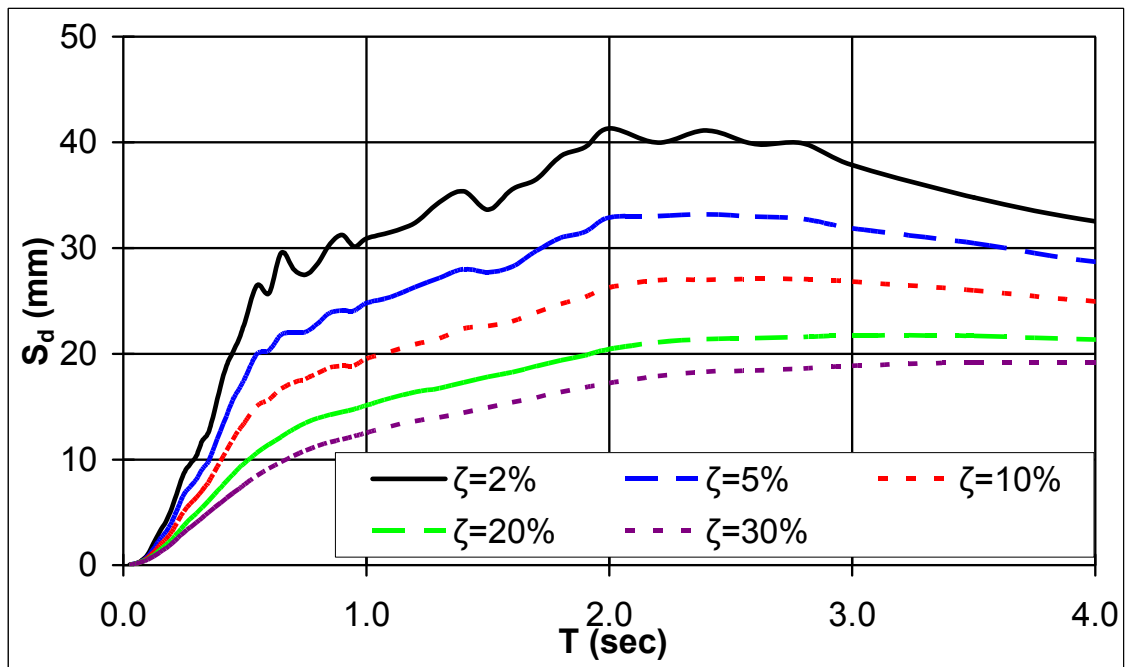


Fig. 2 (b)

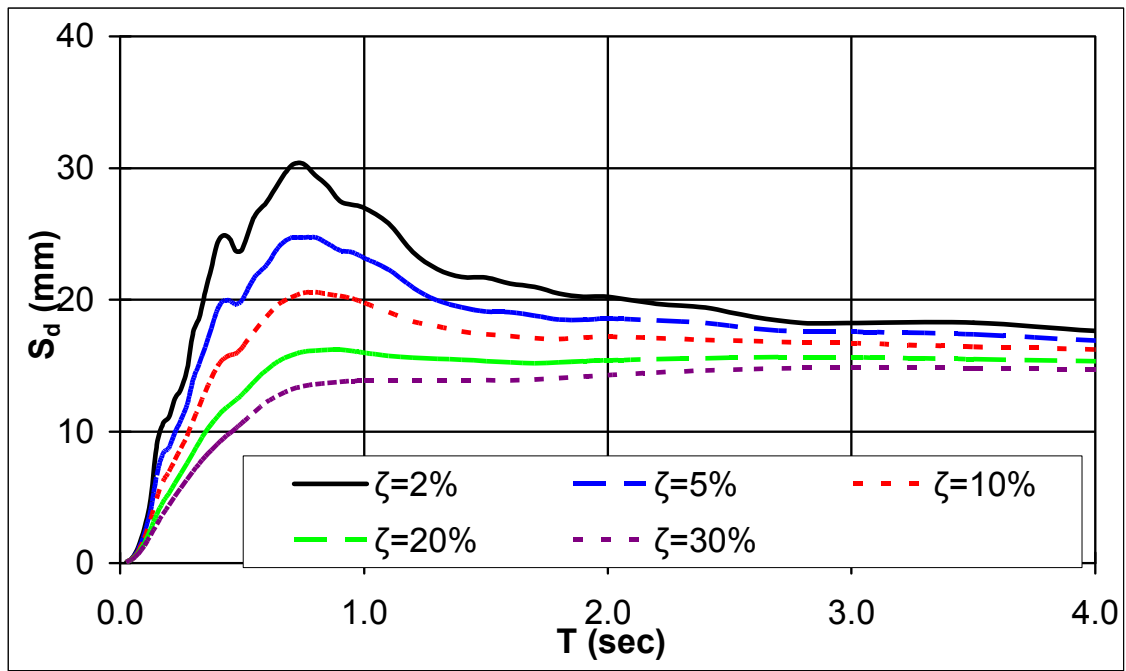


Fig. 2 (c)

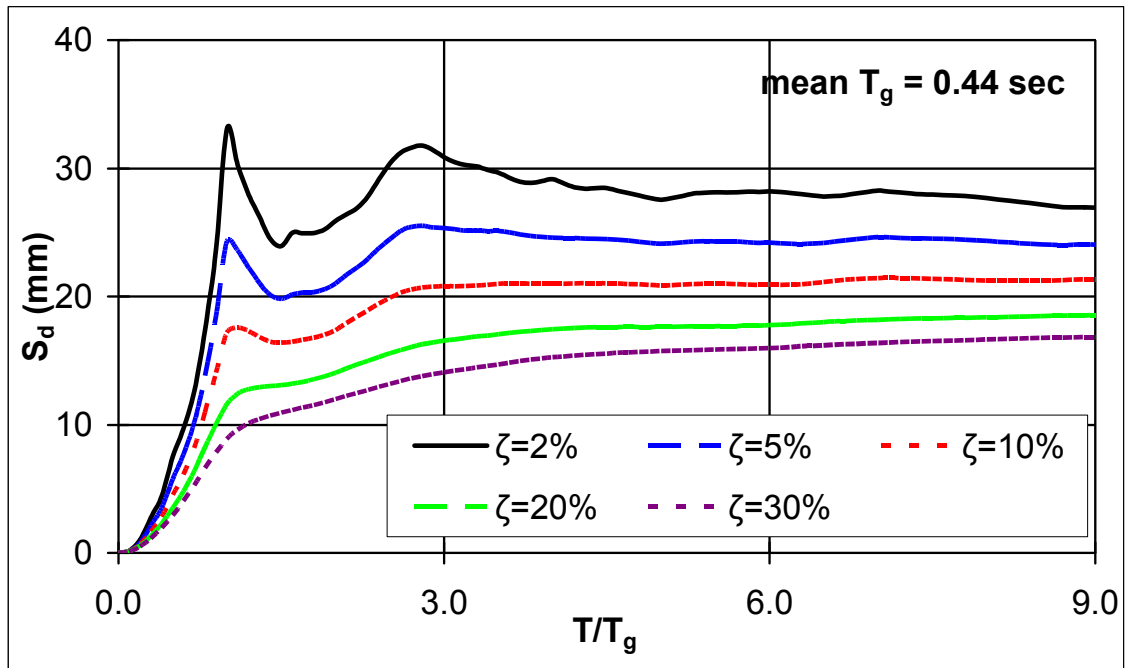


Fig. 3 (a)

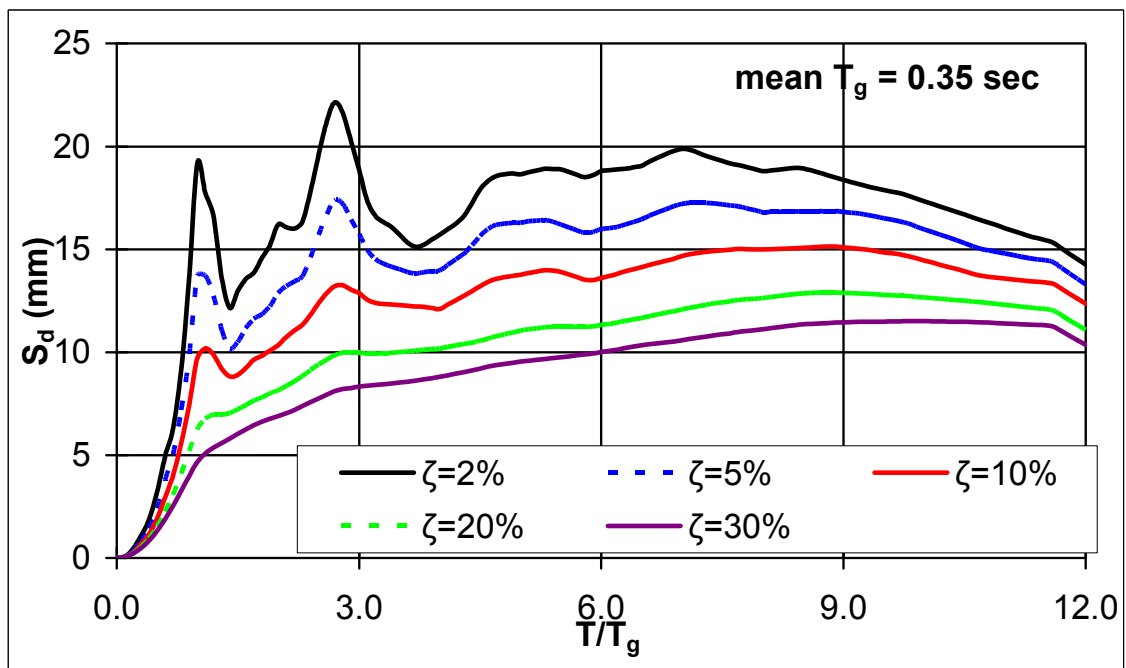


Fig. 3 (b)

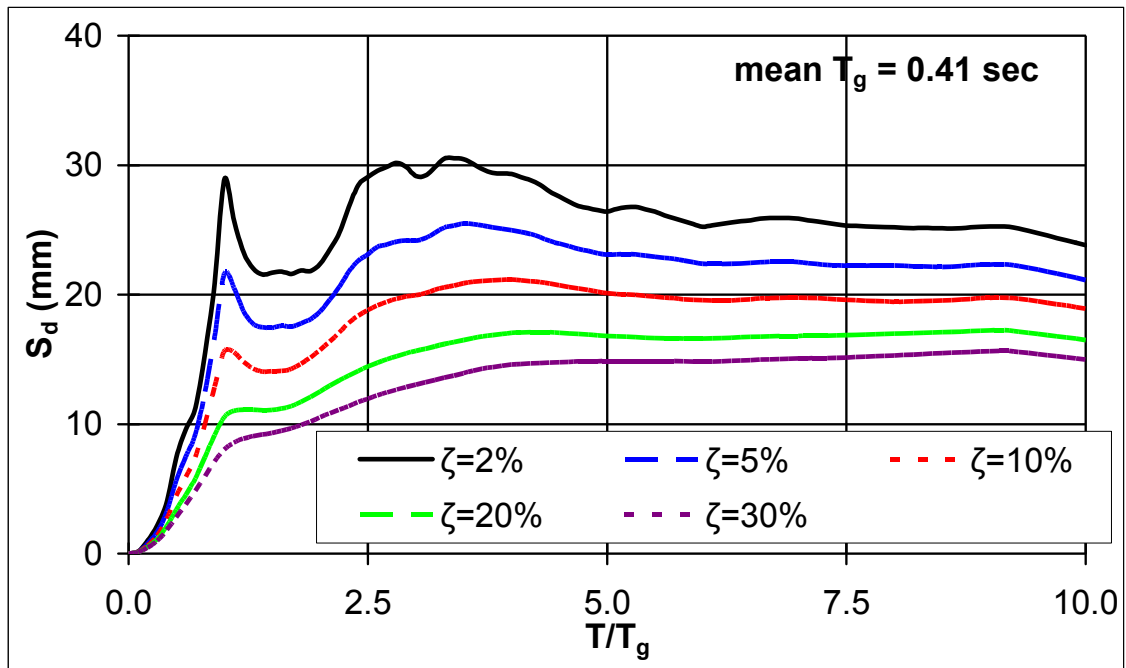


Fig. 3 (c)

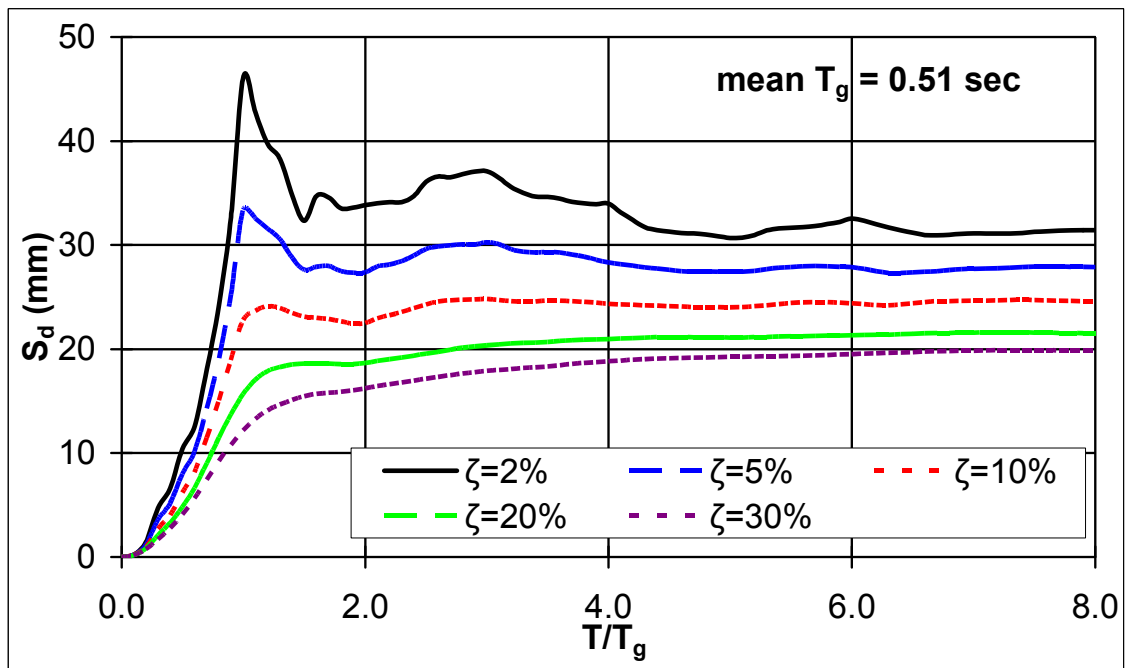


Fig. 3 (d)

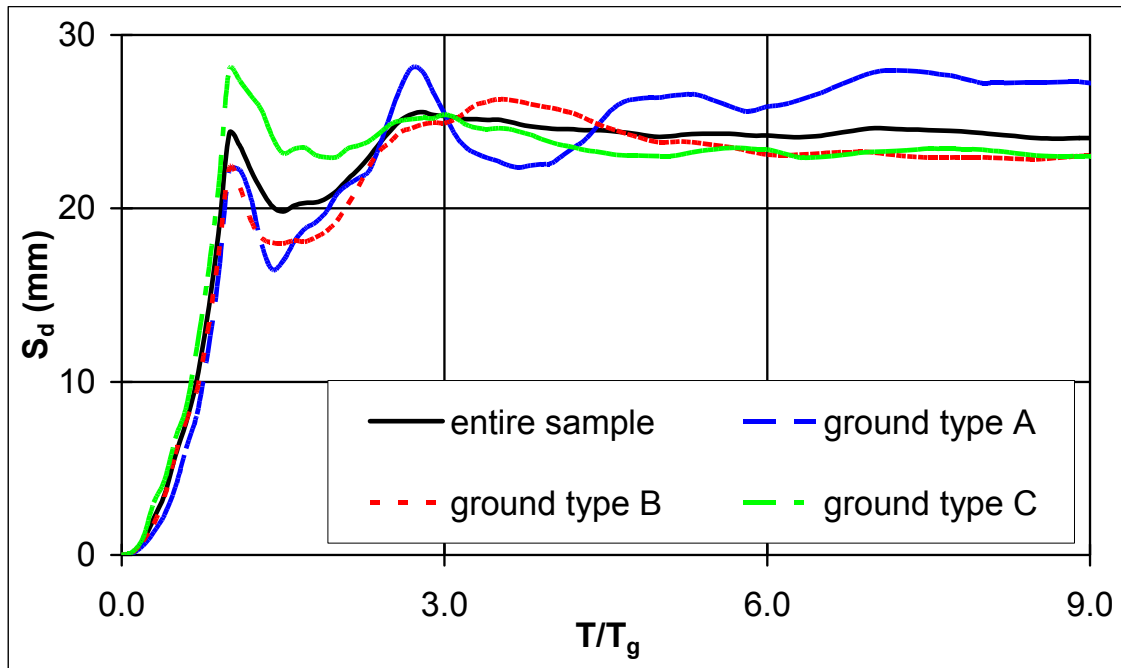


Fig. 4

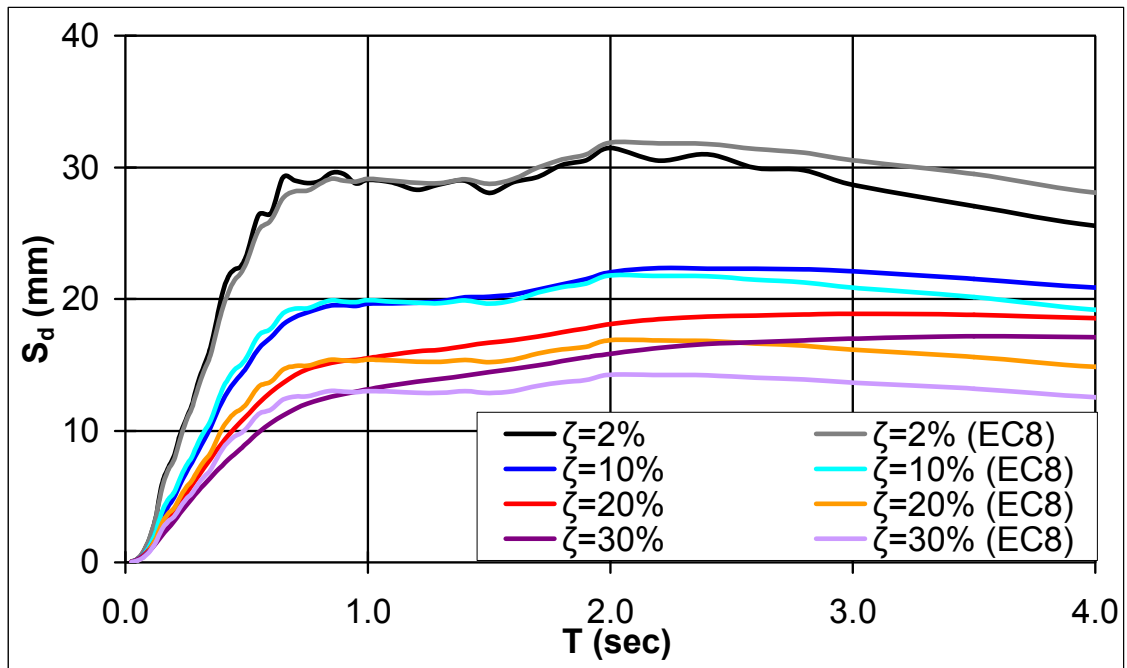


Fig. 5

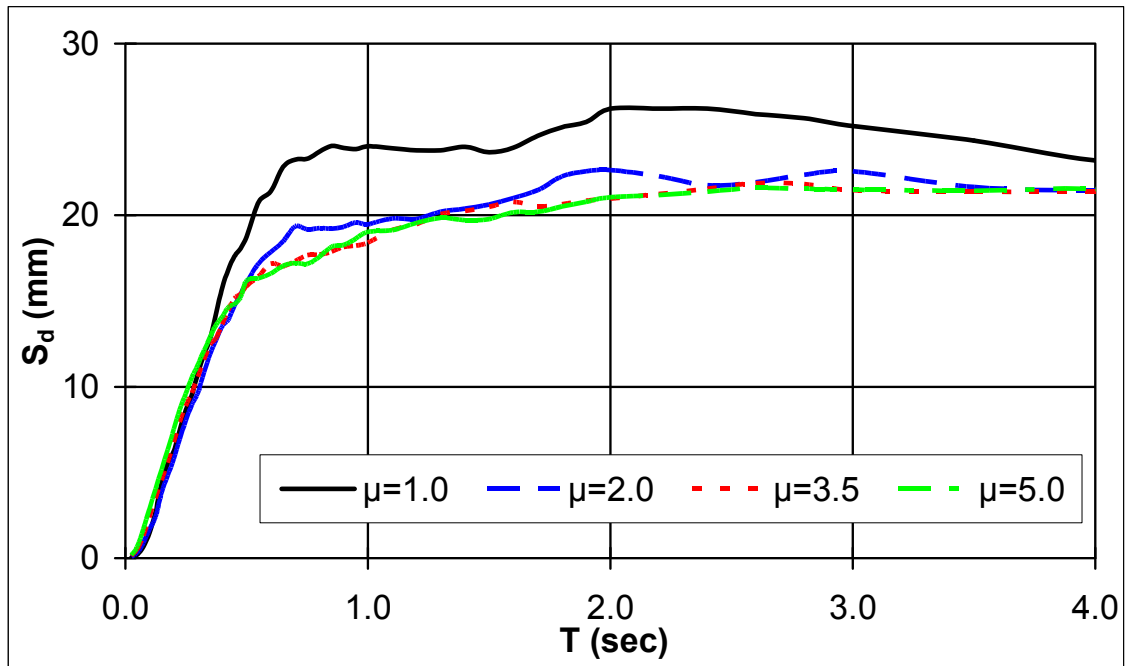


Fig. 6 (a)

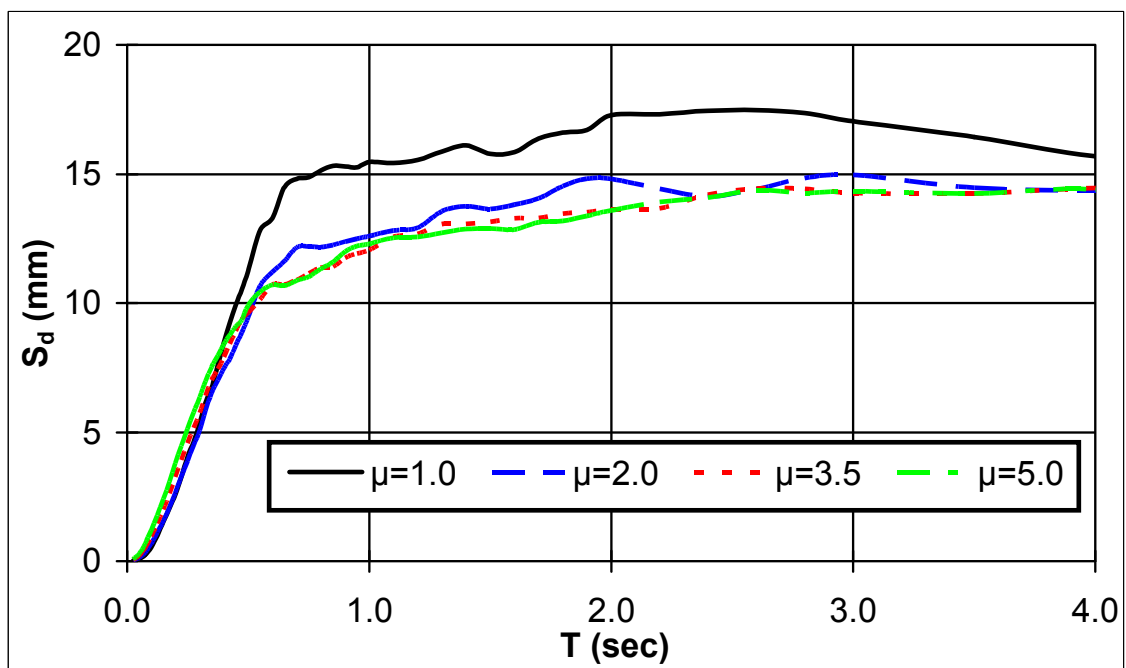


Fig. 6 (b)

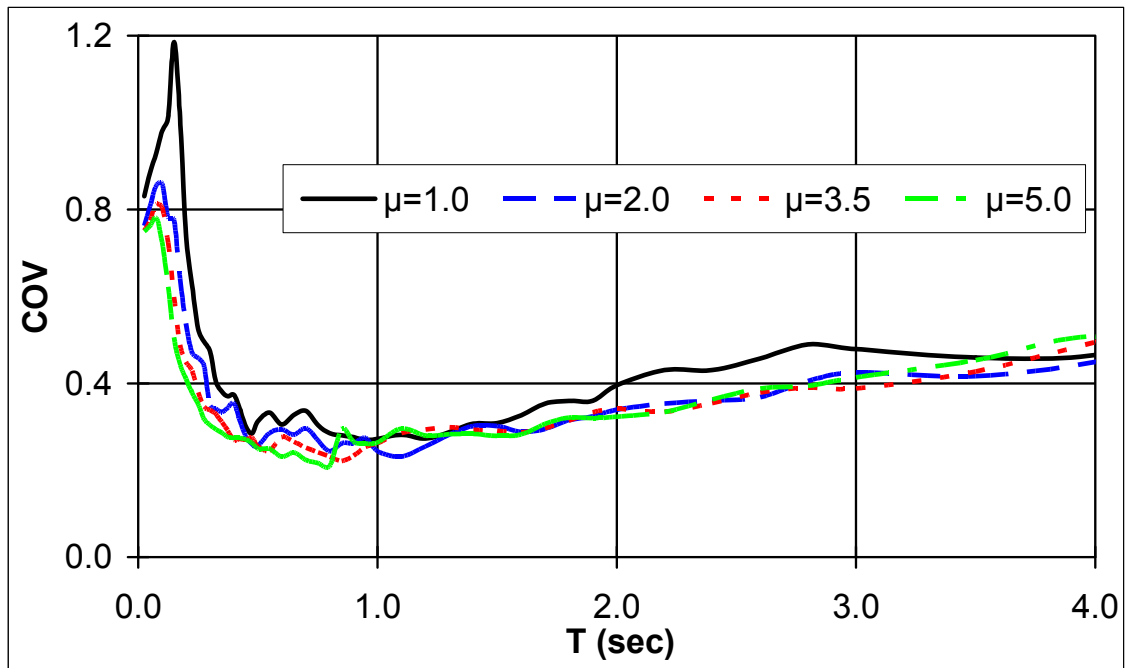


Fig. 6 (c)

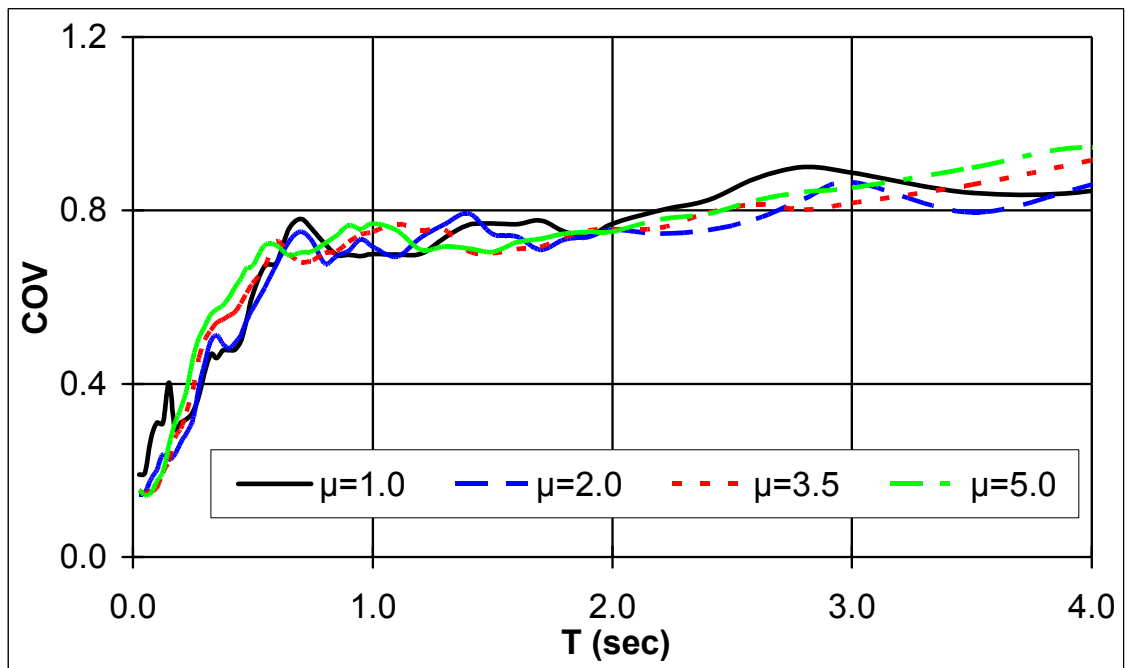


Fig. 6 (d)

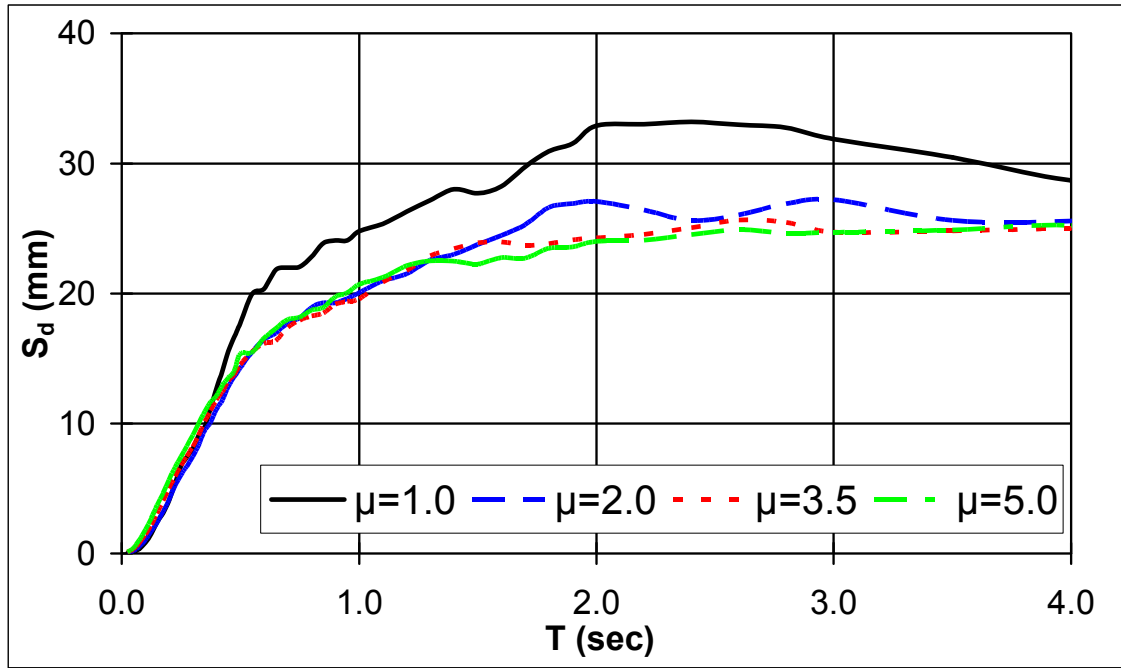


Fig. 7 (a)

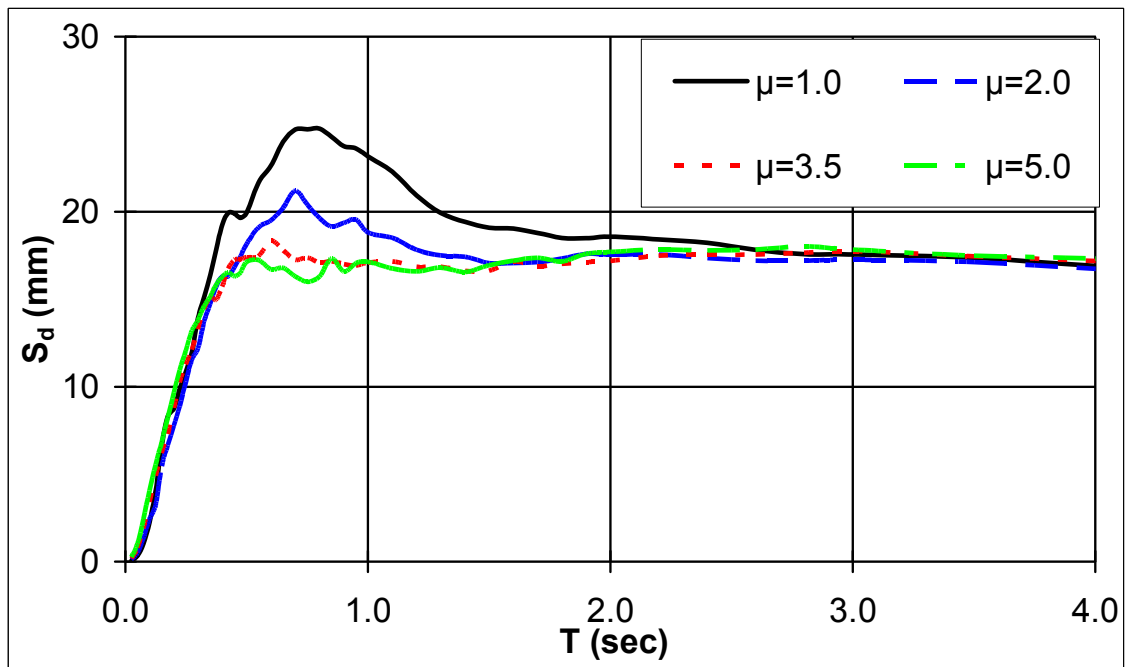


Fig. 7 (b)

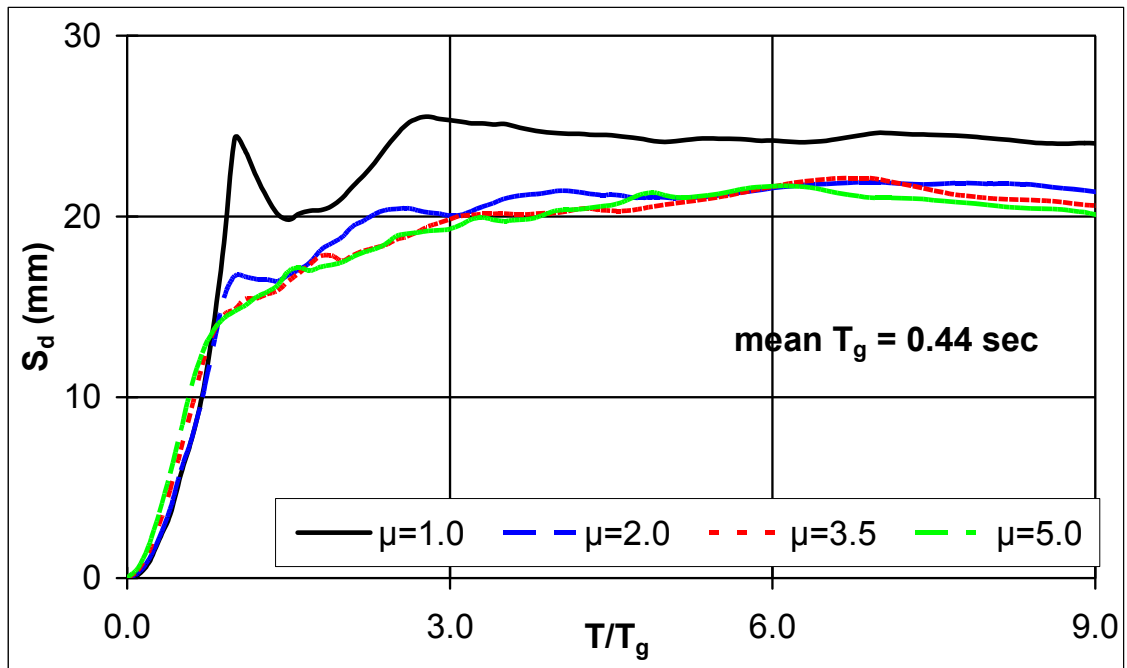


Fig. 8 (a)

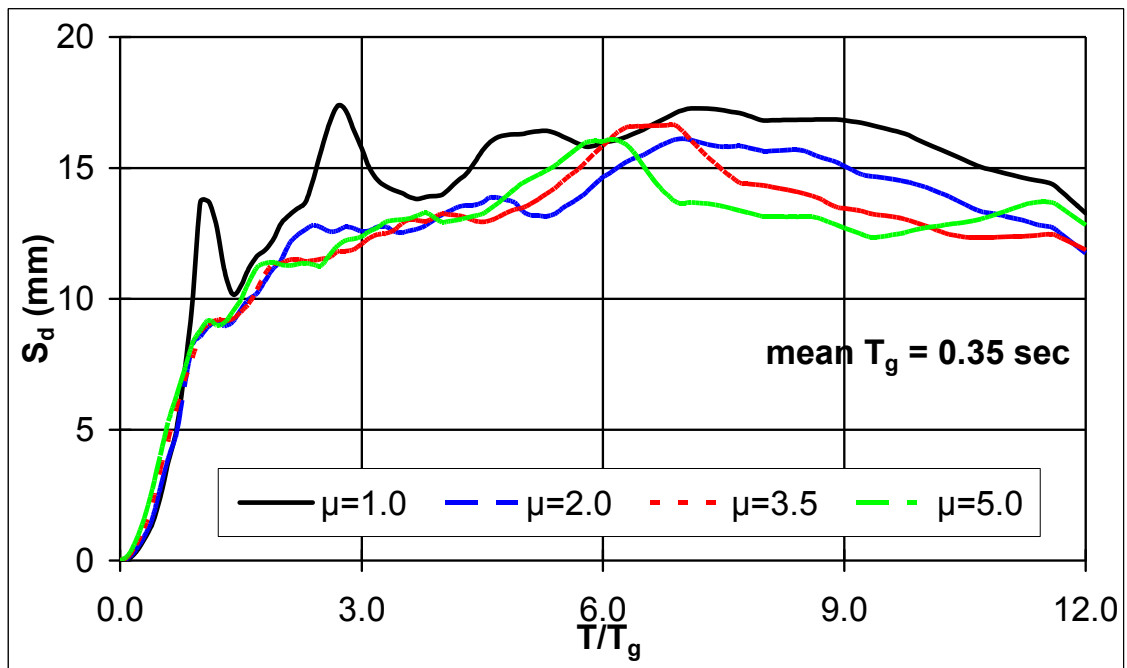


Fig. 8 (b)

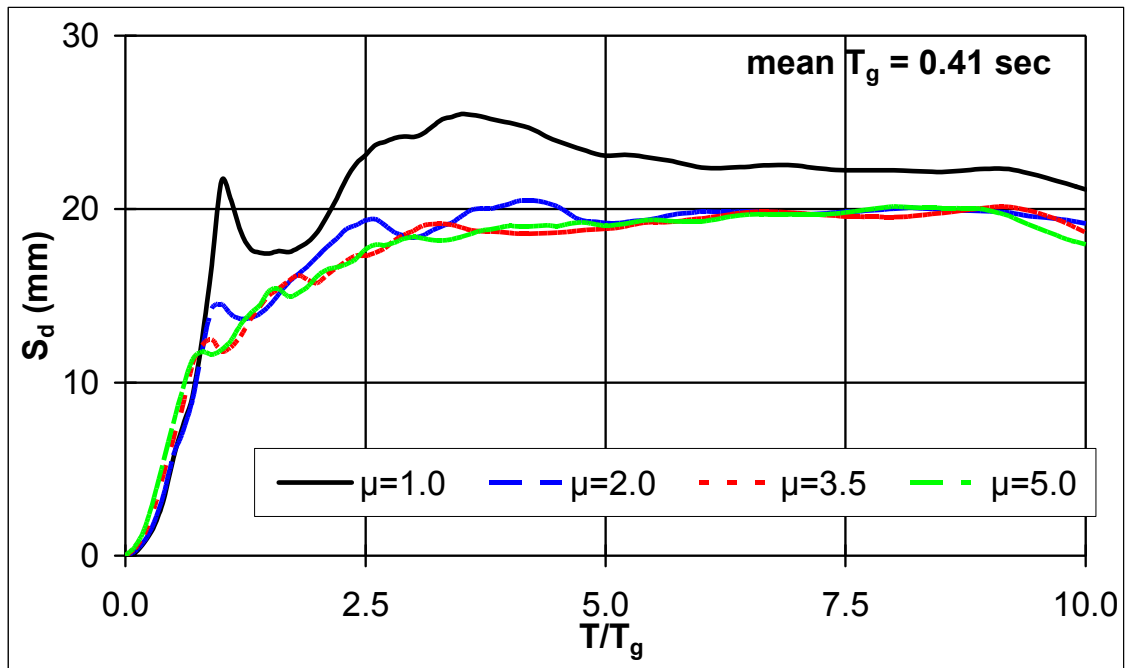


Fig. 8 (c)

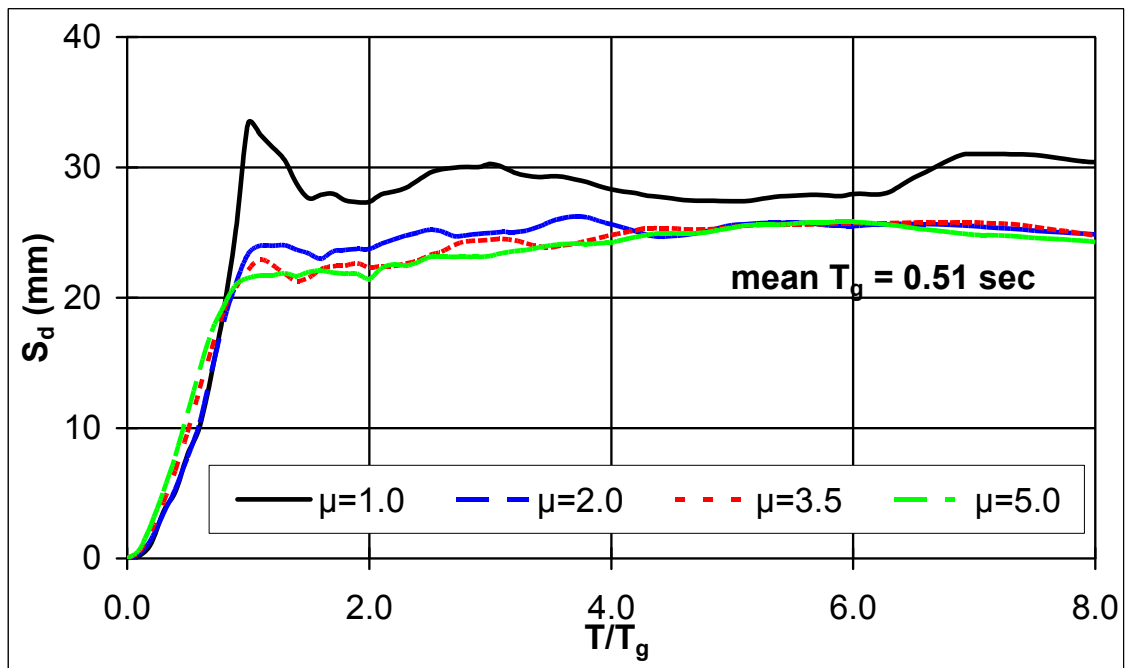


Fig. 8 (d)

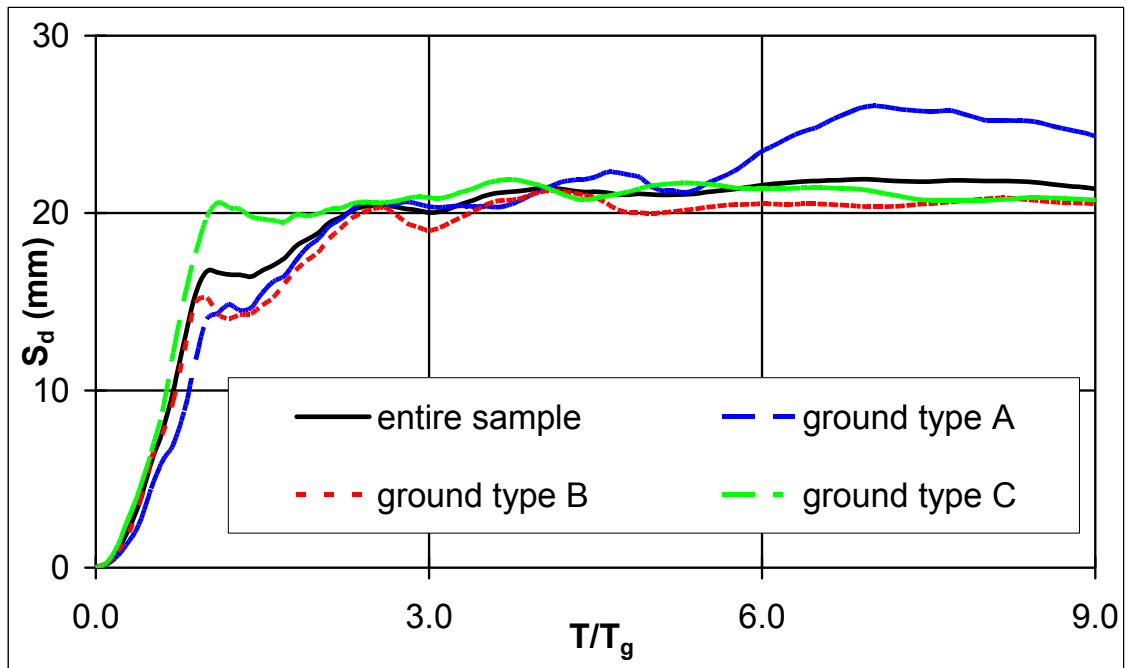


Fig. 9

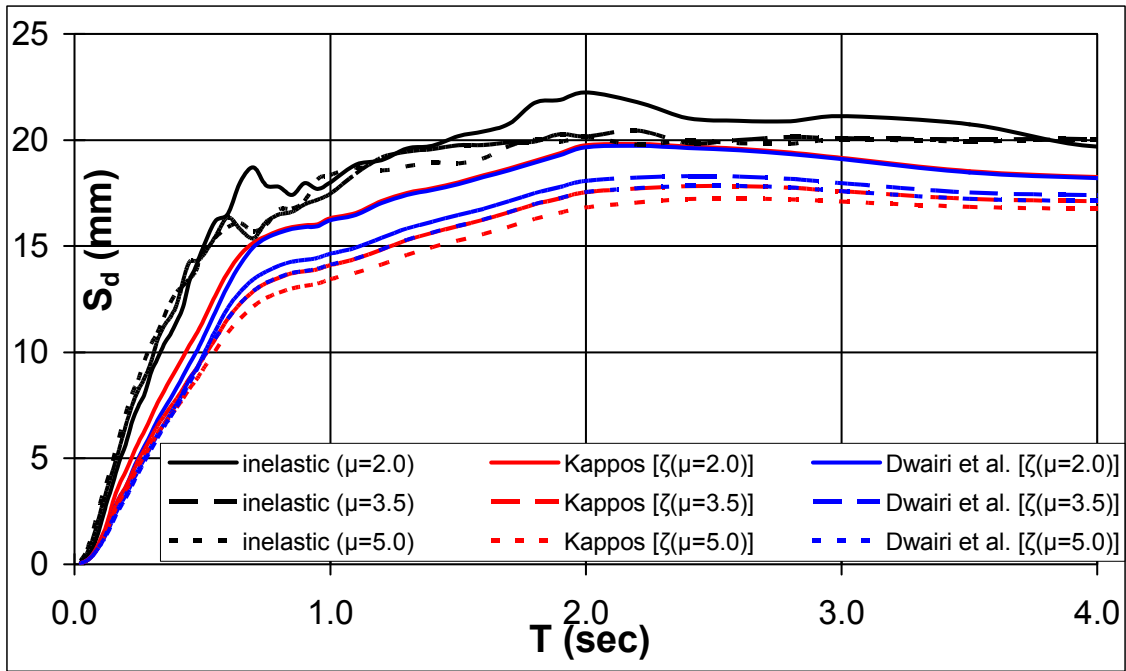


Fig. 10

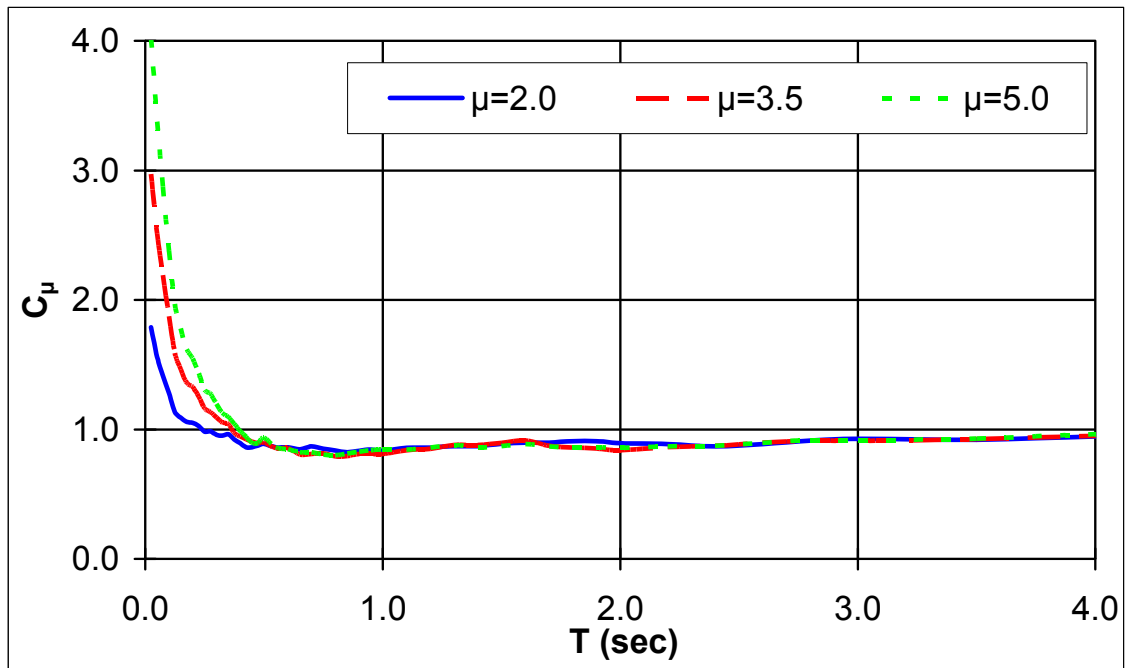


Fig. 11 (a)

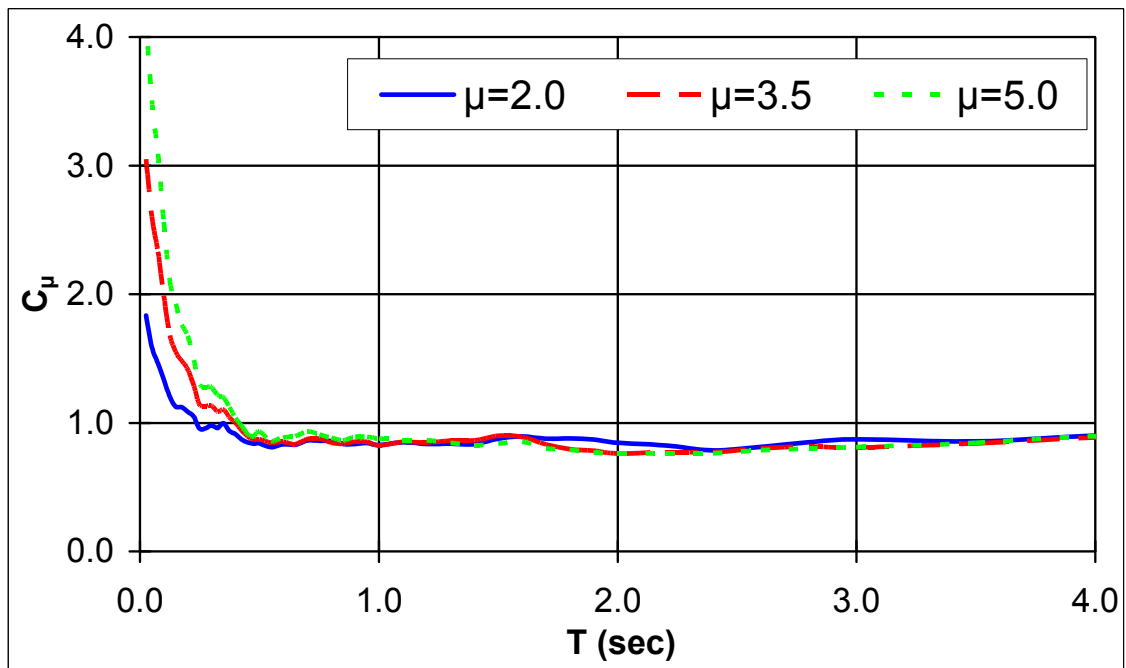


Fig. 11 (b)

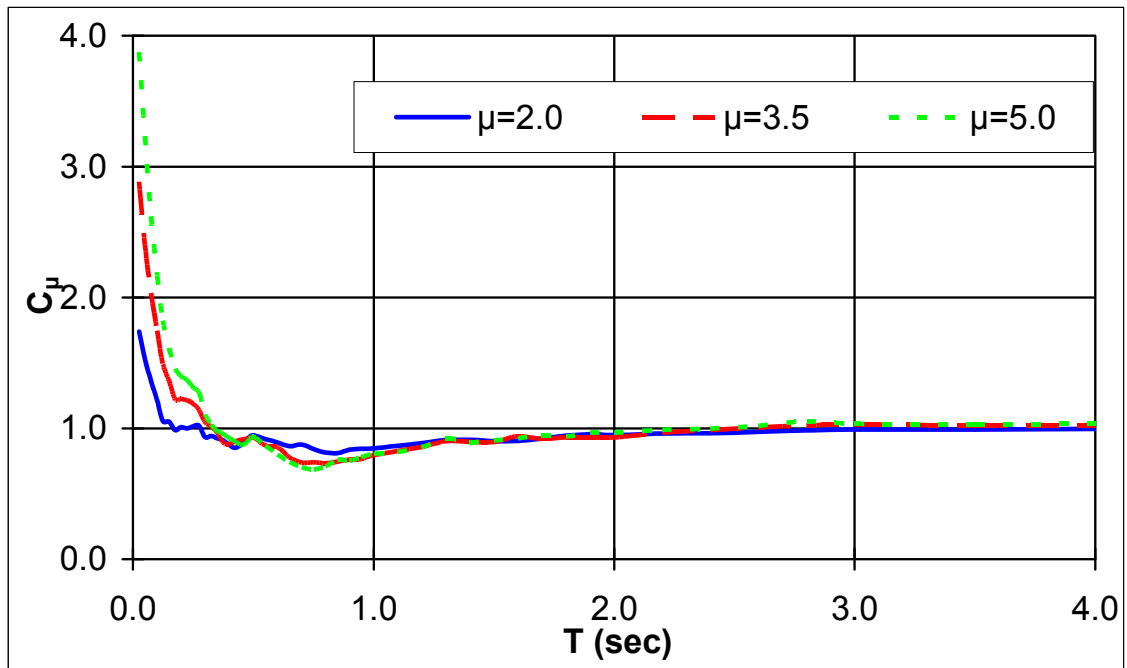


Fig. 11 (c)

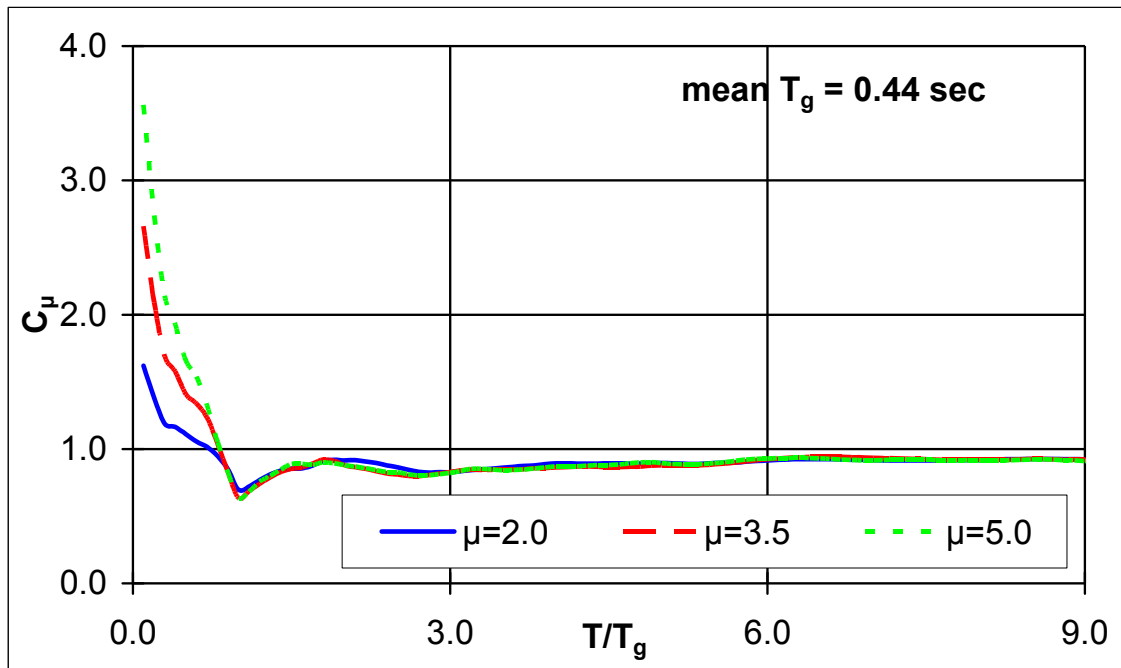


Fig. 12 (a)

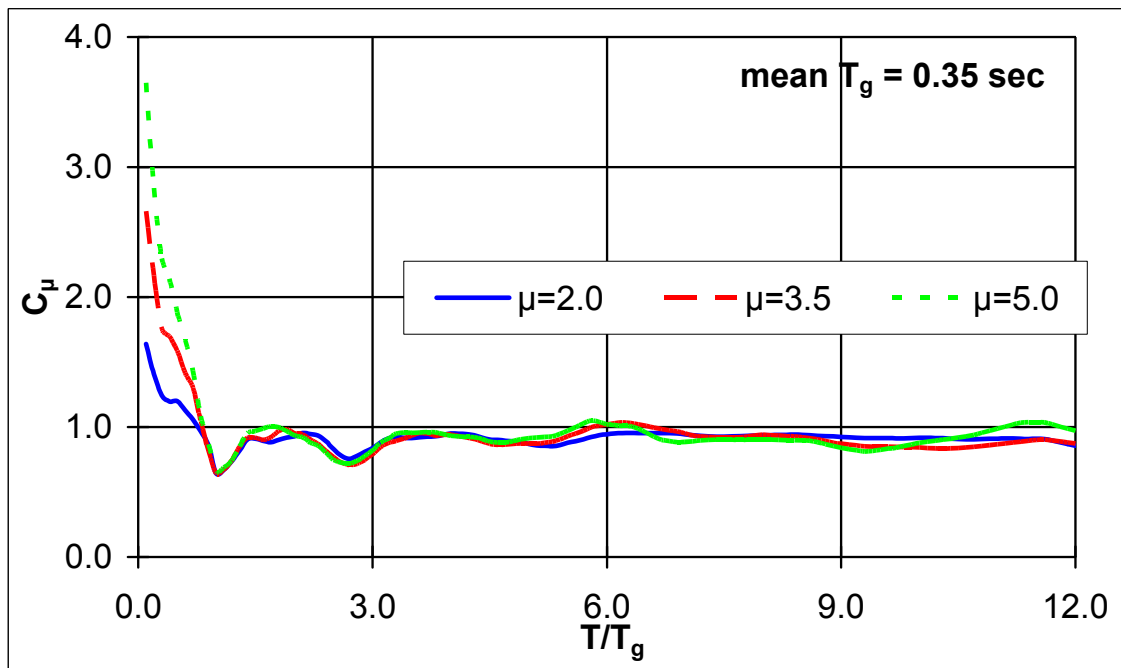


Fig. 12 (b)

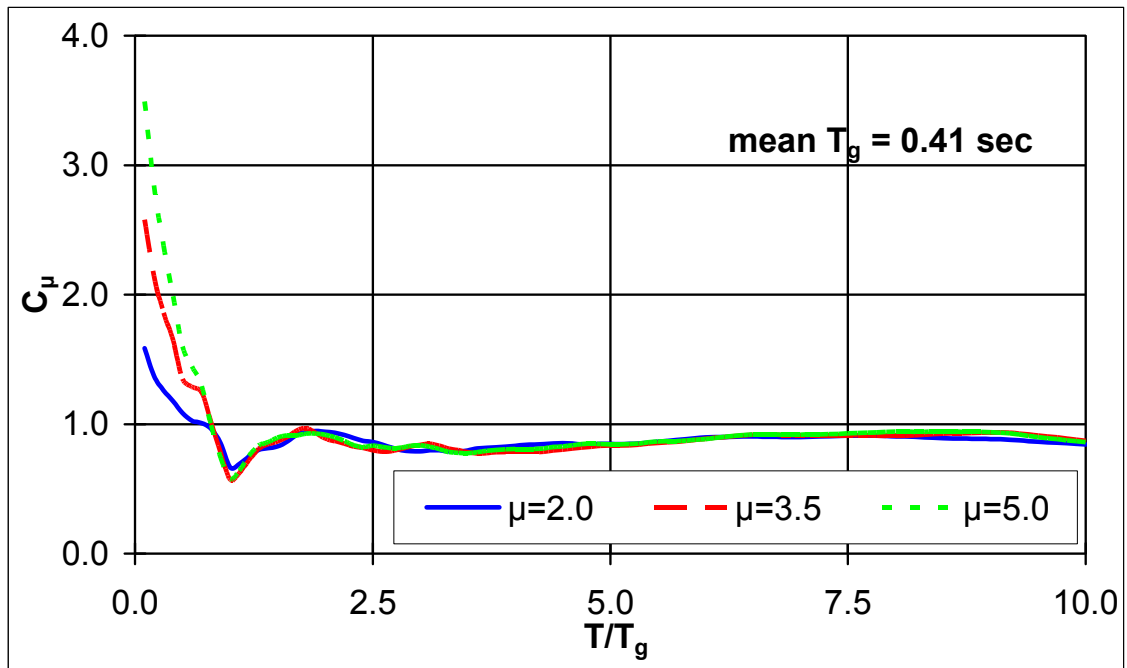


Fig. 12 (c)

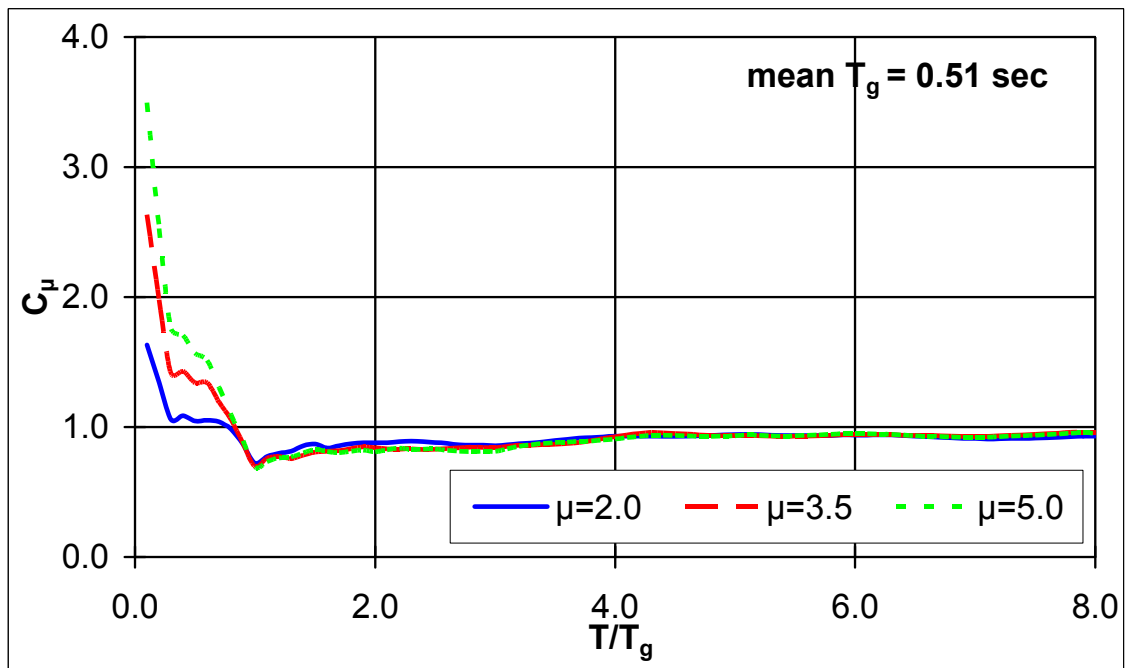


Fig. 12 (d)

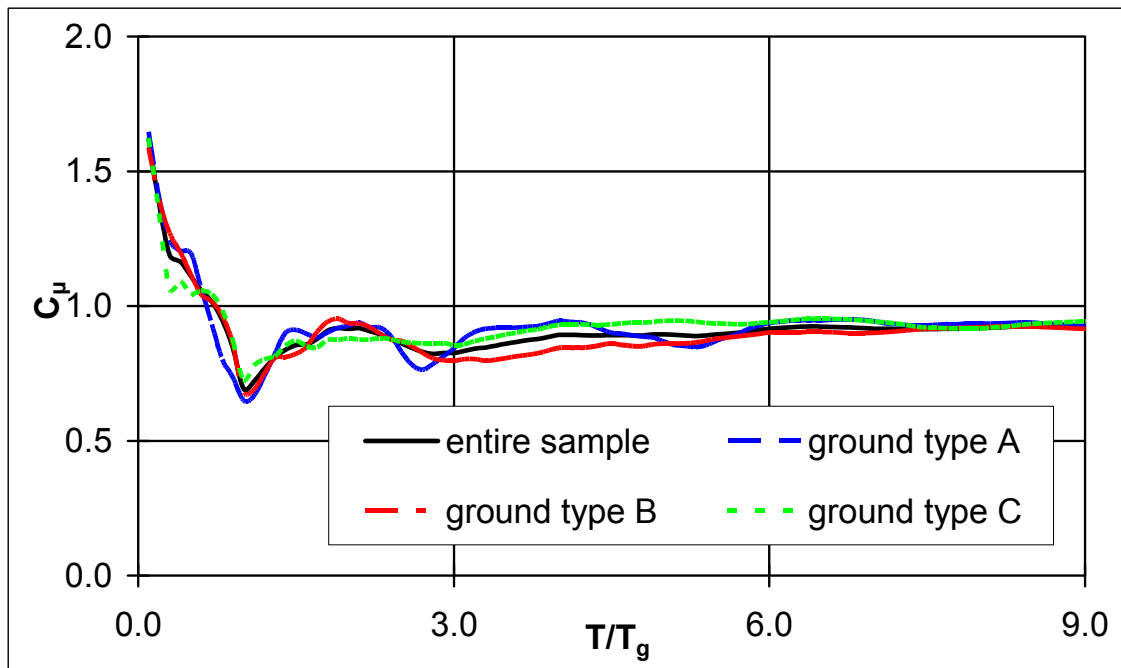


Fig. 13

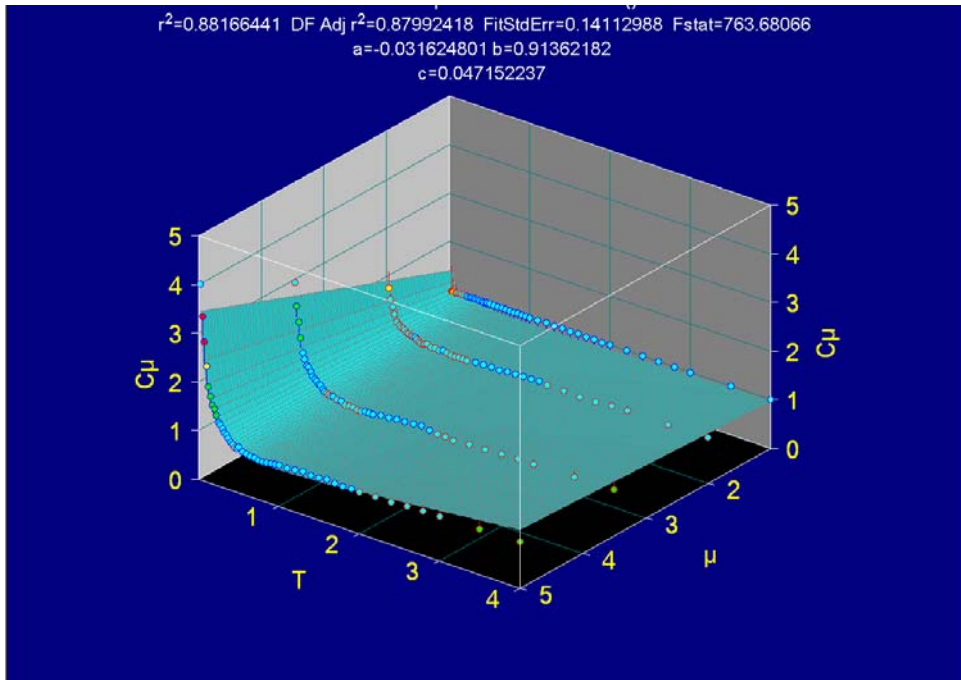


Fig. 14 (a)

Whole sample

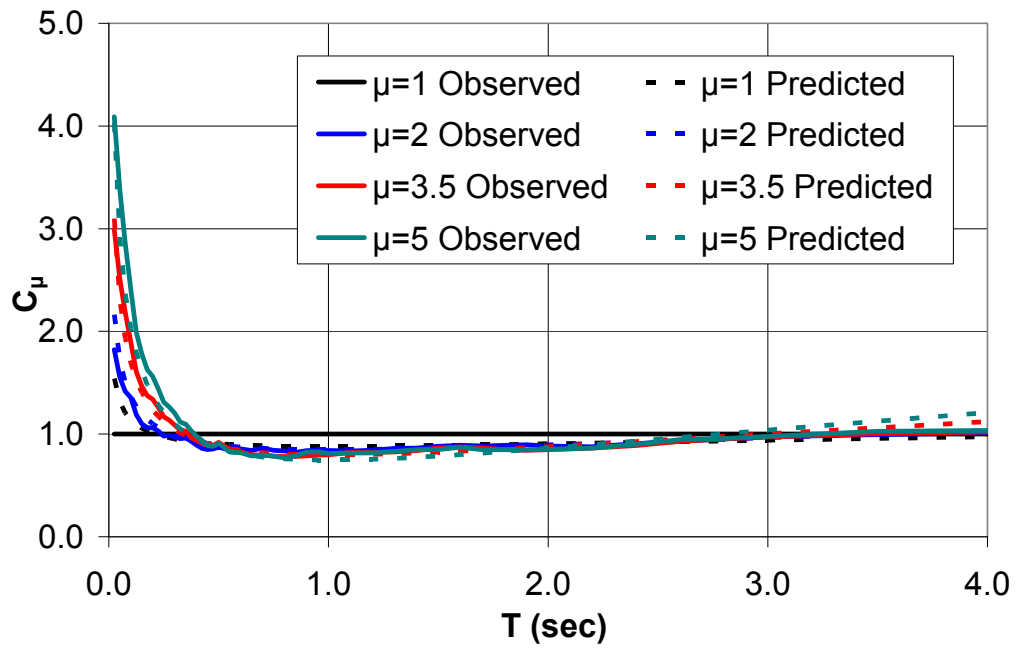


Fig. 14 (b)